

Manuscript version: Author's Accepted Manuscript

The version presented in WRAP is the author's accepted manuscript and may differ from the published version or Version of Record.

Persistent WRAP URL:

<http://wrap.warwick.ac.uk/153861>

How to cite:

Please refer to published version for the most recent bibliographic citation information.

Copyright and reuse:

The Warwick Research Archive Portal (WRAP) makes this work by researchers of the University of Warwick available open access under the following conditions.

Copyright © and all moral rights to the version of the paper presented here belong to the individual author(s) and/or other copyright owners. To the extent reasonable and practicable the material made available in WRAP has been checked for eligibility before being made available.

Copies of full items can be used for personal research or study, educational, or not-for-profit purposes without prior permission or charge. Provided that the authors, title and full bibliographic details are credited, a hyperlink and/or URL is given for the original metadata page and the content is not changed in any way.

Publisher's statement:

Please refer to the repository item page, publisher's statement section, for further information.

For more information, please contact the WRAP Team at: wrap@warwick.ac.uk.

Stability of stainless steel I-section beam-columns at elevated temperatures

Merih Kucukler^{a,*}, Zhe Xing^b, Leroy Gardner^b

^a*School of Engineering, University of Warwick, Coventry, CV4 7AL, UK*

^b*Department of Civil and Environmental Engineering, Imperial College London, London, SW7 2AZ, UK*

Abstract

With the growing use of stainless steel in the construction and offshore industries, there is an increasing interest and need to study the performance of stainless structures at elevated temperatures. The behaviour and design of stainless steel I-section beam-columns in fire is investigated in this paper, addressing a scarcity of previous research on this topic. Finite element (FE) models of stainless steel beam-columns, able to replicate their response at elevated temperatures, are created and validated; the validated models are then used to perform parametric studies to generate extensive benchmark structural performance data. The design rules set out in the European structural steel fire design standard EN 1993-1-2 are assessed and shown to provide rather inaccurate and often unsafe ultimate strength predictions for stainless steel I-section beam-columns in fire. New fire design rules for stainless steel beam-columns are put forward. It is shown that the new proposals are able to offer improved accuracy and design efficiency relative to the EN 1993-1-2 beam-column design rules. The reliability of the proposed design rules is also verified on the basis of the fire design reliability criteria set out by Kruppa [1], thereby demonstrating the suitability of the proposed design rules for inclusion in the upcoming revised version of EN 1993-1-2.

Keywords: Beam-column; Eurocode; Finite element modelling; Fire design; I-section; Stainless steel

1. Introduction

Stainless steel is a high performance structural material that is gaining increasingly widespread use in civil engineering infrastructure, offering enhanced durability and resilience [2]. Despite extensive research into the performance of stainless steel structures at room temperature, there remain gaps in knowledge with respect to their behaviour and design at elevated temperatures. These gaps in knowledge are particularly prominent for the fire performance of stainless steel I-section members, the use of which is becoming increasingly common to satisfy increasing capacity

*Corresponding author

Email addresses: merih.kucukler@warwick.ac.uk (Merih Kucukler), zhe.xing16@imperial.ac.uk (Zhe Xing), leroy.gardner@imperial.ac.uk (Leroy Gardner)

needs, beyond those that can be fulfilled by the conventionally-used cold-formed sections, in more demanding structural applications.

While there have been a number of research studies into the behaviour of stainless steel members under compression [3–9] and bending [10, 11] in fire, relatively few studies have been conducted into the structural response of stainless steel beam-columns at elevated temperatures. Lopes et al. [12, 13] carried out numerical research into the behaviour of stainless steel I-section, square hollow section (SHS) and circular hollow section (CHS) beam-columns in fire. Fan et al. [7] performed two anisothermal fire tests on grade 1.4301 austenitic stainless steel square hollow section beam-columns with critical temperatures in the vicinity of 700 °C. A further series of anisothermal fire tests on rectangular hollow section beam-columns of the same stainless steel grade was also reported in [14], in which three cross-section shapes, three loading eccentricities and critical temperatures ranging between 486 °C and 570 °C were considered. Xing et al. [15] conducted six anisothermal fire tests on grade 1.4301 austenitic stainless steel laser-welded I-section beam-columns with failure temperatures varying from 500 °C to 800 °C. However, a systematic study, considering the full range of contributing parameters to the response of stainless steel beam-columns is yet to be conducted. Building on recent research in which new design rules have been established for the local buckling, flexural buckling and lateral-torsional buckling of stainless steel I-section members [16–18], the aim of the present study is to develop equivalent rules for beam-columns, suitable for incorporation into the next version of EN 1993-1-2 [19].

First, shell finite element models able to replicate the behaviour of stainless steel beam-columns at elevated temperatures are created and validated. Through the validated finite element models, extensive structural performance data, covering austenitic, duplex and ferritic stainless steel grades, a wide range of cross-section geometries, slenderness and elevated temperature levels, are generated for the assessment of the accuracy of the existing EN 1993-1-2 [19] design rules and the development of new fire design rules of stainless steel beam-columns. New beam-column equations, which are consistent with the beam-column provisions set out in the newly revised European standard prEN 1993-1-1 [20] for the room temperature design of steel members, are put forward. The accuracy and reliability of the new proposals are verified against the generated numerical structural performance data and compared to those of the existing beam-column design rules of EN 1993-1-2 [19].

2. Finite element modelling

In this section, finite element models able to mimic the structural response of stainless steel beam-columns in fire are developed and validated against experimental results. The finite element models are then utilised to perform extensive numerical parametric studies, the results of which are used for (i) the assessment of the accuracy of the current EN 1993-1-2 [19] beam-column design rules and (ii) the establishment of a new fire design method for stainless steel I-section beam-columns.

2.1. Development of finite element models

The finite element analysis software Abaqus [21] was employed in this study to perform the numerical simulations of the structural response of stainless steel I-section beam-columns at elevated temperatures. The four-noded reduced integration general purpose shell finite element S4R,

which has been successfully used for similar previous applications [22–24], was employed to create all the finite element models. Shell elements were used in favour of beam elements to ensure that both local and global instability effects could be explicitly captured in the models. To accurately replicate the cross-section and member behaviour of stainless steel beam-columns, sixteen elements were used to model each constituent flange and web plate and the element numbers along the member lengths were determined such that the element aspect ratios within the web plates were approximately equal to unity [25].

The two-stage Ramberg–Osgood (R–O) material model [26–28] was used to define the elevated temperature stress-strain ($\sigma - \varepsilon$) response of stainless steel in the finite element models, as adopted by [16, 17], and given by eqs. (1) and (2):

$$\varepsilon = \frac{\sigma}{E_\theta} + 0.002 \left(\frac{\sigma}{f_{p0.2,\theta}} \right)^{n_\theta} \quad \text{for } \sigma \leq f_{p0.2,\theta}, \quad (1)$$

$$\varepsilon = \frac{\sigma - f_{p0.2,\theta}}{E_{p0.2,\theta}} + \left(\varepsilon_{u,\theta} - \varepsilon_{p0.2,\theta} - \frac{f_{u,\theta} - f_{p0.2,\theta}}{E_{p0.2,\theta}} \right) \left(\frac{\sigma - f_{p0.2,\theta}}{f_{u,\theta} - f_{p0.2,\theta}} \right)^{m_\theta} + \varepsilon_{p0.2,\theta} \quad \text{for } f_{p0.2,\theta} < \sigma \leq f_{u,\theta}, \quad (2)$$

where E_θ is the Young's modulus at temperature θ , $f_{p0.2,\theta}$ is the 0.2% proof strength at temperature θ , $E_{p0.2,\theta}$ is the tangent modulus corresponding to $f_{p0.2,\theta}$, $\varepsilon_{p0.2,\theta}$ is the total strain corresponding to $f_{p0.2,\theta}$, $f_{u,\theta}$ is the ultimate tensile strength at temperature θ , $\varepsilon_{u,\theta}$ is the ultimate strain at temperature θ and n_θ and m_θ are strain hardening exponents. To ensure that the second stage of the R-O material model passes through $f_{2,\theta}$ and $f_{u,\theta}$ exactly at the 2% total strain and the ultimate strain $\varepsilon_{u,\theta}$ [16, 17, 29] (see Fig. 1), the values of strain hardening exponent m_θ were calculated as:

$$m_\theta = \frac{\ln \left(\frac{0.02 - \varepsilon_{p0.2,\theta} - \frac{f_{2,\theta} - f_{p0.2,\theta}}{E_{p0.2,\theta}}}{\varepsilon_{u,\theta} - \varepsilon_{p0.2,\theta} - \frac{f_{u,\theta} - f_{p0.2,\theta}}{E_{p0.2,\theta}}} \right)}{\ln \left(\frac{f_{2,\theta} - f_{p0.2,\theta}}{f_{u,\theta} - f_{p0.2,\theta}} \right)} \quad \text{but } 1.50 \leq m_\theta \leq 5.00. \quad (3)$$

The elevated temperature material strengths ($f_{p0.2,\theta}$, $f_{2,\theta}$, and $f_{u,\theta}$) and ultimate strain ($\varepsilon_{u,\theta}$) in eqs. (1) and (2) were determined by multiplying the standardised room temperature material properties (f_y , f_u and ε_u) established for hot-rolled stainless steel plates in [30], which are shown in Table 1, by the corresponding strength ($k_{p0.2,\theta}$, $k_{2,\theta}$, $k_{u,\theta}$) and ductility ($k_{\varepsilon_{u,\theta}}$) reduction factors recommended in the SCI Structural Stainless Steel Design Manual [31], i.e. $f_{p0.2,\theta} = k_{p0.2,\theta} f_y$, $f_{2,\theta} = k_{2,\theta} f_y$, $f_{u,\theta} = k_{u,\theta} f_u$, and $\varepsilon_{u,\theta} = k_{\varepsilon_{u,\theta}} \varepsilon_u$. The elevated temperature Young's moduli E_θ were determined by multiplying the room temperature Young's modulus of 200 GPa by the stiffness reduction factors ($k_{E,\theta}$) given in [31], while the elevated temperature strain hardening exponents n_θ used in the R-O material model were taken as the same as those proposed to define the room temperature material response n in [30]. The elevated temperature strength and stiffness reduction factors given in [31]

are shown in Fig. 3 for the (a) austenitic, (b) duplex and (c) ferritic stainless steel grades considered in this paper; those for carbon steel taken from [19] are also displayed for comparison in Fig. 3 (d). Comparisons of the adopted material stress-strain curves for the considered austenitic, duplex and ferritic stainless steel grades for different temperature levels against those for carbon steel determined according to EN 1993-1-2 [19] are shown Fig. 4.

The boundary conditions applied to the finite element models of the beam-columns under major axis bending plus axial compression and those subjected to minor axis bending plus axial compression are illustrated in Fig. 5. As can be seen from the figure, the displacements and rotations of the end cross-sections were linked to two reference points, referred to as RP1 and RP2, through rigid body kinematic coupling constraints. The horizontal and vertical translations (U1 and U2) and rotation about axis 3 (UR3) of the two reference points, as well as the longitudinal translation (U3) of reference point 2 (i.e. RP2), were restrained. For the models of the beam-columns under major axis bending plus axial compression (see Fig. 5(a)), the horizontal translations (U1) at the web-flange junctions were also restrained along the member lengths to ensure in-plane buckling of the beam-columns; out-of-plane buckling of stainless steel I-section beam-columns in fire will be explored in a future study. The forces were applied as concentrated axial loads and bending moments to the two reference points, as shown in Fig. 5.

All the beam-columns modelled in this study were assumed to be fabricated by the welding of individual hot-rolled stainless steel plates, and hence the residual stress pattern proposed by Yuan et al. [32] for welded stainless steel I-sections, which is shown in Fig. 7, was adopted. As can be seen from the figure, the peak tensile residual stresses in the flanges (σ_{ft}) and web (σ_{wt}) were taken as 80% of the room temperature yield strength f_y , taken as the 0.2% proof strength (i.e. $f_y = f_{p0.2}$), for austenitic stainless steel I-sections (i.e. $\sigma_{ft} = \sigma_{wt} = 0.8f_y$), while the peak tensile residual stresses in the flanges σ_{ft} and web σ_{wt} were taken as 60% of the room temperature yield strength f_y for duplex and ferritic stainless steel I-sections (i.e. $\sigma_{ft} = \sigma_{wt} = 0.6f_y$). The peak compressive residual stresses in the flanges (σ_{fc}) and web (σ_{wc}) were determined on the basis of axial force equilibrium, as described in Yuan et al. [32].

In the numerical simulations carried out in this paper, the finite element models of the stainless steel beam-columns in fire were analysed isothermally, utilising the following three steps. In the first step, the residual stresses were applied to the models in conjunction with the corresponding residual plastic strains $\varepsilon_{res,pl}$, as recommended in [17, 33]. Considering the nonlinear stress-strain response of stainless steel defined through the R-O material model given in eqs. (1) and (2), the residual plastic strains $\varepsilon_{res,pl}$ at the cross-section integration points were determined from:

$$\varepsilon_{res,pl} = 0.002 \left(\frac{\sigma_{res}}{f_y} \right)^n, \quad (4)$$

where σ_{res} is the residual stress magnitude applied at each cross-section integration point. Note that due to the nonlinear stress-strain response of stainless steel, the application of the residual plastic strains $\varepsilon_{res,pl}$ to the models is necessary to ensure the precise implementation of the residual stress pattern of [32] shown in Fig. 7. Omission of the residual plastic strains would result in a redistribution of stresses and a different residual stress pattern at the end of the first step from that applied and intended. Following the attainment of self-equilibrium in the finite element models within the first step, the temperature of the finite element models was increased uniformly to the

target temperature value θ in the second step, resulting in the development of thermal strains in the models and the modification of their material response as shown in Fig. 1. In the final step, Geometrically and Materially Nonlinear Analyses with Imperfections (GMNIA) were performed using the modified Riks method to trace the full load-deformation response, where the peak loads were taken as the ultimate load-carrying capacities of the stainless steel beam-columns in fire.

2.2. Validation of finite element models

The six fire tests carried out by Xing et al. [15] on austenitic stainless steel I-section beam-columns were utilised to validate the adopted finite element modelling approach. The measured geometric properties and imperfections of the six beam-columns were employed in the validation study. Sixteen elements were utilised across the width of each web and flange plate of the modelled I-sections; the element number along the member length was then determined by adopting an element aspect ratio of unity. The two-stage R-O material model given by eqs. (1) and (2) was used to define the elevated temperature stress-strain response of the specimens, using the elevated temperature material properties determined by multiplying the strength and stiffness reduction factors given in [31] by the room temperature material properties obtained from the tensile coupon tests performed by Xing et al. [15]. The three analysis steps described in Section 2.1 were adopted in the validation of the finite element modelling approach, taking the target temperatures θ equal to the critical temperature θ_{cr} values measured in the fire tests. The numerically determined failure loads $N_{Ed,FE}$ are compared against those obtained from the fire tests $N_{Ed,test}$ in Table 2, where it can be seen that the ratios of the failure loads determined using the finite element models $N_{Ed,FE}$ to those observed in the tests $N_{Ed,test}$ are generally close to unity, thus verifying that the finite element models created in this study are able to accurately predict the ultimate resistances of stainless steel beam-columns in fire. Excellent agreement is also obtained in comparisons between the experimental and FE failure modes, typical examples of which are shown in Fig. 2.

2.3. Parametric studies

Numerical parametric studies were conducted to establish comprehensive data for the structural response of stainless steel I-section beam-columns at elevated temperatures. The range of the parameters explored in the numerical studies are summarised in Table 3, where it can be seen that three stainless steel grades: (i) grade 1.4301 austenitic stainless steel, (ii) grade 1.4462 duplex stainless steel and (iii) grade 1.4003 ferritic stainless steel were considered and, for each grade, six cross-section profiles were modelled. The chosen profiles covered all four cross-section classes according to both the room temperature and elevated temperature cross-section classification criteria set out in EN 1993-1-4 [34] and EN 1993-1-2 [19], respectively. The considered elevated temperature levels varied from 200 °C to 800 °C in increments of 200 °C, while the considered elevated temperature non-dimensional slendernesses $\bar{\lambda}_\theta$ of the beam-columns equal to the square root of the ratio of the axial yield load Af_y to the elastic critical flexural buckling load N_{cr} multiplied by the square root of the ratio of the strength and stiffness reduction factors $\sqrt{k_{2,\theta}/k_{E,\theta}}$ (i.e. $\bar{\lambda}_\theta = \sqrt{Af_y/N_{cr}} \sqrt{k_{2,\theta}/k_{E,\theta}}$) were 0.5, 1 and 1.5 (i.e. $\bar{\lambda}_\theta = 0.5, 1.0$ and 1.5). Note that for the beam-columns under combined major axis bending and compression, the non-dimensional slendernesses were taken as the major axis flexural buckling slendernesses $\bar{\lambda}_{y,\theta}$ determined using the major axis elastic flexural buckling loads $N_{cr,y}$ ($\bar{\lambda}_\theta = \bar{\lambda}_{y,\theta} = \sqrt{Af_y/N_{cr,y}} \sqrt{k_{2,\theta}/k_{E,\theta}}$), while for those under

minor axis bending plus axial compression, the non-dimensional slendernesses $\bar{\lambda}_\theta$ were taken as the minor axis flexural buckling slendernesses $\bar{\lambda}_{z,\theta}$ determined using the minor axis elastic flexural buckling loads $N_{cr,z}$ ($\bar{\lambda}_\theta = \bar{\lambda}_{z,\theta} = \sqrt{A f_y / N_{cr,z}} \sqrt{k_{2,\theta} / k_{E,\theta}}$). In the numerical parametric studies, a parameter referred to as the radial angle ϕ was used to describe the combination of axial compression and bending moment applied to a beam-column; the radial angle ϕ is calculated as:

$$\phi = \tan^{-1} \left(\frac{N_{Ed} / N_{Rd}}{M_{Ed} / M_{Rd}} \right), \quad (5)$$

where N_{Rd} and M_{Rd} are the axial compression resistance and bending moment resistance calculated using the considered design method. The definition of the radial angle ϕ within a beam-column interaction curve is illustrated in Fig. 8. As can be seen from the figure, when the radial angle ϕ increases from 0° to 90° , the applied loading changes from pure bending ($\phi = 0^\circ$) to combined axial compression and bending ($0^\circ < \phi < 90^\circ$), and then to pure compression ($\phi = 90^\circ$). In the numerical parametric studies, six different radial angles ϕ , varying from 0° to 90° , were considered for each beam-column at each elevated temperature level θ , as shown in Table 3. Fig. 9 shows typical failure modes of stainless steel beam-columns under major axis bending plus axial compression and under minor axis bending plus axial compression.

3. Assessment of existing EN 1993-1-2 design rules for stainless steel beam-columns in fire

According to EN 1993-1-2 [19], a stainless steel member subjected to combined axial compression and bending in fire should satisfy eqs. (6)–(7) when it has a Class 1 or Class 2 cross-section:

$$\frac{N_{fi,Ed}}{\chi_{min,fi} A k_{y,\theta} \frac{f_y}{\gamma_{M,fi}}} + \frac{k_y M_{y,fi,Ed}}{W_{pl,y} k_{y,\theta} \frac{f_y}{\gamma_{M,fi}}} + \frac{k_z M_{z,fi,Ed}}{W_{pl,z} k_{y,\theta} \frac{f_y}{\gamma_{M,fi}}} \leq 1, \quad (6)$$

$$\frac{N_{fi,Ed}}{\chi_{z,fi} A k_{y,\theta} \frac{f_y}{\gamma_{M,fi}}} + \frac{k_{LT} M_{y,fi,Ed}}{\chi_{LT,fi} W_{pl,y} k_{y,\theta} \frac{f_y}{\gamma_{M,fi}}} + \frac{k_z M_{z,fi,Ed}}{W_{pl,z} k_{y,\theta} \frac{f_y}{\gamma_{M,fi}}} \leq 1, \quad (7)$$

eqs. (8)–(9) when it has a Class 3 cross-section:

$$\frac{N_{fi,Ed}}{\chi_{min,fi} A k_{y,\theta} \frac{f_y}{\gamma_{M,fi}}} + \frac{k_y M_{y,fi,Ed}}{W_{el,y} k_{y,\theta} \frac{f_y}{\gamma_{M,fi}}} + \frac{k_z M_{z,fi,Ed}}{W_{el,z} k_{y,\theta} \frac{f_y}{\gamma_{M,fi}}} \leq 1, \quad (8)$$

$$\frac{N_{fi,Ed}}{\chi_{z,fi} A k_{y,\theta} \frac{f_y}{\gamma_{M,fi}}} + \frac{k_{LT} M_{y,fi,Ed}}{\chi_{LT,fi} W_{el,y} k_{y,\theta} \frac{f_y}{\gamma_{M,fi}}} + \frac{k_z M_{z,fi,Ed}}{W_{el,z} k_{y,\theta} \frac{f_y}{\gamma_{M,fi}}} \leq 1, \quad (9)$$

and eqs. (10)–(11) when it has a Class 4 cross-section:

$$\frac{N_{\text{fi,Ed}}}{\chi_{\text{min,fi}} A_{\text{eff}} k_{y,\theta} \frac{f_y}{\gamma_{\text{M,fi}}}} + \frac{k_y M_{y,\text{fi,Ed}}}{W_{\text{eff,y}} k_{y,\theta} \frac{f_y}{\gamma_{\text{M,fi}}}} + \frac{k_z M_{z,\text{fi,Ed}}}{W_{\text{eff,z}} k_{y,\theta} \frac{f_y}{\gamma_{\text{M,fi}}}} \leq 1, \quad (10)$$

$$\frac{N_{\text{fi,Ed}}}{\chi_{z,\text{fi}} A_{\text{eff}} k_{y,\theta} \frac{f_y}{\gamma_{\text{M,fi}}}} + \frac{k_{\text{LT}} M_{y,\text{fi,Ed}}}{\chi_{\text{LT,fi}} W_{\text{eff,y}} k_{y,\theta} \frac{f_y}{\gamma_{\text{M,fi}}}} + \frac{k_z M_{z,\text{fi,Ed}}}{W_{\text{eff,z}} k_{y,\theta} \frac{f_y}{\gamma_{\text{M,fi}}}} \leq 1. \quad (11)$$

In eqs. (6)–(11), $N_{\text{fi,Ed}}$ is the design axial force, $M_{y,\text{fi,Ed}}$ and $M_{z,\text{fi,Ed}}$ are the maximum major axis and minor axis first order bending moments along the length of the beam-column, $\chi_{\text{min,fi}}$ is the lowest of the buckling reduction factors determined for flexural buckling about the major and minor axes, torsional buckling and torsional-flexural buckling, $\chi_{z,\text{fi}}$ is the lowest of the buckling reduction factors determined for flexural buckling about the minor axis, torsional buckling and torsional-flexural buckling and $\chi_{\text{LT,fi}}$ is the reduction factor for lateral-torsional buckling. For the geometric properties, A and A_{eff} are the gross cross-sectional area and the effective area, $W_{\text{pl,y}}$, $W_{\text{el,y}}$ and $W_{\text{eff,y}}$ are the plastic, elastic and effective section moduli about the major axis and $W_{\text{pl,z}}$, $W_{\text{el,z}}$ and $W_{\text{eff,z}}$ are the plastic, elastic and effective section moduli about the minor axis; for the material properties, $k_{y,\theta}$ is the yield strength reduction factor taken as $k_{2,\theta}$ for members with Class 1, 2 or 3 cross-sections and $k_{p0.2,\theta}$ for members with Class 4 cross-sections and f_y is the yield strength (i.e. the 0.2% proof strength) at room temperature. Finally, $\gamma_{\text{M,fi}}$ is the partial safety factor for fire design taken as 1.0 and k_y , k_z and k_{LT} are interaction coefficients calculated as:

$$k_y = 1 - \frac{\mu_y N_{\text{fi,Ed}}}{\chi_{y,\text{fi}} A k_{y,\theta} \frac{f_y}{\gamma_{\text{M,fi}}}} \leq 3 \quad (12)$$

with $\mu_y = (2\beta_{\text{M,y}} - 5)\bar{\lambda}_{y,\theta} + 0.44\beta_{\text{M,y}} + 0.29 \leq 0.8$,

$$k_z = 1 - \frac{\mu_z N_{\text{fi,Ed}}}{\chi_{z,\text{fi}} A k_{y,\theta} \frac{f_y}{\gamma_{\text{M,fi}}}} \leq 3 \quad (13)$$

with $\mu_z = (1.2\beta_{\text{M,z}} - 3)\bar{\lambda}_{z,\theta} + 0.71\beta_{\text{M,z}} - 0.29 \leq 0.8$,

$$k_{\text{LT}} = 1 - \frac{\mu_{\text{LT}} N_{\text{fi,Ed}}}{\chi_{z,\text{fi}} A k_{y,\theta} \frac{f_y}{\gamma_{\text{M,fi}}}} \leq 1 \quad (14)$$

with $\mu_{\text{LT}} = 0.15\bar{\lambda}_{z,\theta}\beta_{\text{M,LT}} - 0.15 \leq 0.9$, where $\beta_{\text{M,y}}$ and $\beta_{\text{M,z}}$ are equivalent uniform moment factors. Note that $k_{2,\theta}$ is the elevated temperature reduction factor for the strength at 2% total strain, which is equal to the ratio of the elevated temperature strength at 2% total strain $f_{2,\theta}$ to the room temperature yield strength (i.e. $k_{2,\theta} = f_{2,\theta}/f_y$), while $k_{p0.2,\theta}$ is the elevated temperature 0.2% proof

strength reduction factor equal to the ratio of the elevated temperature 0.2% proof strength $f_{p0.2,\theta}$ to the room temperature yield strength (i.e. $k_{p0.2,\theta} = f_{p0.2,\theta}/f_y$).

Using the column and beam buckling design curves for the determination of $\chi_{\min,fi}$, $\chi_{z,fi}$ and $\chi_{LT,fi}$ and the effective width rules for the determination of the effective section properties A_{eff} , $W_{eff,y}$ and $W_{eff,z}$ given in EN 1993-1-2 [19], the accuracy of the existing beam-column design rules of EN 1993-1-2 [19] is assessed against the results from the nonlinear finite element modelling, considering the wide range of parameters set out in Table 3. Figs. 10–12 show the assessment of the accuracy of the current EN 1993-1-2 [19] beam-column design equations against the GMNIA results for beam-columns subjected to uniform major axis bending plus compression and having the same cross-section properties as those of a European HEM 200 cross-section for the austenitic stainless steel members, an HEB 300 cross-section for the duplex stainless steel members and an HEAA 180 cross-section for the ferritic stainless steel members. In the figures, N_{pl} and $M_{y,pl}$ are the elevated temperature axial force and plastic major axis bending moment resistances determined considering the gross cross-section properties and the elevated temperature strengths at 2% total strains $f_{2,\theta}$ (i.e. $N_{pl} = Af_{2,\theta}$ and $M_{y,pl} = W_{pl,y}f_{2,\theta}$). The interaction curves are plotted based on the design resistances calculated according to the classification of the presented cross-section under the varying combination of axial force and bending moment. It can be seen from Figs. 10–12 that the current EN 1993-1-2 [19] rules lead to somewhat inaccurate ultimate strength predictions for stainless steel I-section beam-columns in fire that lie generally on the unsafe side. Similar results are found for the cases where the beam-columns were subjected to minor axis bending plus axial compression (see Figs. 13–15 in which $M_{z,pl} = W_{pl,z}f_{2,\theta}$), thus indicating the need to develop a new fire design approach for stainless steel beam-columns.

4. Development of new proposals for the design of stainless steel beam-columns in fire

The development of the new fire design rules for stainless steel beam-columns is described in this section. In the development of the proposed design rules, the format used in the beam-column design approach of the upcoming version of the European standard for room temperature structural steel design prEN 1993-1-1 [20] was adopted with the aim of increasing consistency between two standards. This is also in line with the recently developed design rules for stainless steel beam-columns at room temperature [42–46]. In addition to this, the elevated temperature strength at 2% total strain $f_{2,\theta} = k_{2,\theta}f_y$ was adopted in the new proposals for the design of stainless steel beam-columns in fire with cross-sections falling into all the cross-section classes to ensure consistency with the recently revised fire design rules for carbon steel beam-columns in [35], which will appear in the next version of EN 1993-1-2 [19].

4.1. New proposals for the design of stainless steel beam-columns in fire

In the new beam-column design rules proposed in this study, the cross-sections are classified into two classes: (i) ‘non-slender’ and (ii) ‘slender’ in line with the cross-section classification approach developed in Xing et al. [16]. The design buckling resistance of members with non-slender cross-sections subjected to combined axial compression and bending in fire should thus

satisfy eqs. (15)–(16):

$$\frac{N_{fi,Ed}}{\chi_{y,fi} A k_{2,\theta} \frac{f_y}{\gamma_{M,fi}}} + k_{yy} \frac{M_{y,fi,Ed}}{W_{pl,y} k_{2,\theta} \frac{f_y}{\gamma_{M,fi}}} + k_{yz} \frac{M_{z,fi,Ed}}{W_{pl,z} k_{2,\theta} \frac{f_y}{\gamma_{M,fi}}} \leq 1, \quad (15)$$

$$\frac{N_{fi,Ed}}{\chi_{z,fi} A k_{2,\theta} \frac{f_y}{\gamma_{M,fi}}} + k_{zy} \frac{M_{y,fi,Ed}}{\chi_{LT,fi} W_{pl,y} k_{2,\theta} \frac{f_y}{\gamma_{M,fi}}} + k_{zz} \frac{M_{z,fi,Ed}}{W_{pl,z} k_{2,\theta} \frac{f_y}{\gamma_{M,fi}}} \leq 1. \quad (16)$$

For members with slender cross-sections, eqs. (17)–(18) should be satisfied:

$$\frac{N_{fi,Ed}}{\chi_{y,fi} A_{eff} k_{2,\theta} \frac{f_y}{\gamma_{M,fi}}} + k_{yy} \frac{M_{y,fi,Ed} + \Delta M_{y,fi,Ed}}{W_{eff,y} k_{2,\theta} \frac{f_y}{\gamma_{M,fi}}} + k_{yz} \frac{M_{z,fi,Ed} + \Delta M_{z,fi,Ed}}{W_{eff,z} k_{2,\theta} \frac{f_y}{\gamma_{M,fi}}} \leq 1, \quad (17)$$

$$\frac{N_{fi,Ed}}{\chi_{z,fi} A_{eff} k_{2,\theta} \frac{f_y}{\gamma_{M,fi}}} + k_{zy} \frac{M_{y,fi,Ed} + \Delta M_{y,fi,Ed}}{\chi_{LT,fi} W_{eff,y} k_{2,\theta} \frac{f_y}{\gamma_{M,fi}}} + k_{zz} \frac{M_{z,fi,Ed} + \Delta M_{z,fi,Ed}}{W_{eff,z} k_{2,\theta} \frac{f_y}{\gamma_{M,fi}}} \leq 1, \quad (18)$$

where $\Delta M_{y,fi,Ed}$ and $\Delta M_{z,fi,Ed}$ are the moments due to the shift of the centroid of the effective cross-section relative to that of the gross cross-section, $\chi_{y,fi}$ is the buckling reduction factor considering flexural buckling about the major axis and $\chi_{z,fi}$ is the minimum of the buckling reduction factors for minor axis flexural buckling, torsional or torsional-flexural buckling; the determination of $\chi_{y,fi}$ and $\chi_{z,fi}$ using the newly derived column buckling curves for stainless steel members in fire is described in [25]. Additionally, $\chi_{LT,fi}$ is the reduction factor for lateral-torsional buckling, which may be taken as $\chi_{LT,fi} = 1.0$ for beam-columns that are not susceptible (either due to the cross-section shape or the provision of sufficiently closely spaced lateral restraints) to flexural-torsional buckling. Note that the proposals made herein will be extended in future work to the flexural-torsional buckling assessment of stainless steel I-section beam-columns in fire, considering the lateral-torsional buckling curves derived in [18] for stainless steel I-section beams at elevated temperatures. It should also be emphasised that in the proposed method considered currently the effective section properties A_{eff} , $W_{eff,y}$ and $W_{eff,z}$ of the stainless steel beam-columns should be determined on the basis of the new effective width rules established in Xing et al. [16, 36] for stainless steel cross-sections in fire.

In eqs. (15)–(18), k_{yy} , k_{yz} , k_{zy} and k_{zz} are the interaction factors for the design of members with doubly symmetric cross-sections. The interaction factor k_{yy} is calculated as:

$$k_{yy} = C_{my} \left[1 + D_{1,y} (\bar{\lambda}_{y,\theta} - D_{2,y}) n_y \right] \quad \text{for } \bar{\lambda}_{y,\theta} < D_{3,y}, \quad (19)$$

$$k_{yy} = C_{my} \left[1 + D_{1,y} (D_{1,y} - D_{3,y}) n_y \right] \quad \text{for } \bar{\lambda}_{y,\theta} \geq D_{3,y}, \quad (20)$$

and the interaction factor k_{zz} is determined as:

$$k_{zz} = C_{mz} \left[1 + D_{1,z} (\bar{\lambda}_{z,\theta} - D_{2,z}) n_z \right] \quad \text{for } \bar{\lambda}_{z,\theta} < D_{3,z}, \quad (21)$$

$$k_{zz} = C_{mz} \left[1 + D_{1,z} (D_{3,z} - D_{2,z}) n_z \right] \quad \text{for } \bar{\lambda}_{z,\theta} \geq D_{3,z}, \quad (22)$$

in which the parameters n_y and n_z are calculated using the following equations:

$$n_y = \frac{N_{fi,Ed}}{\chi_{y,fi} A k_{2,\theta} \frac{f_y}{\gamma_{M,fi}}} \quad \text{and} \quad n_z = \frac{N_{fi,Ed}}{\chi_{z,fi} A k_{2,\theta} \frac{f_y}{\gamma_{M,fi}}} \quad \text{for non-slender sections,} \quad (23)$$

$$n_y = \frac{N_{fi,Ed}}{\chi_{y,fi} A_{eff} k_{2,\theta} \frac{f_y}{\gamma_{M,fi}}} \quad \text{and} \quad n_z = \frac{N_{fi,Ed}}{\chi_{z,fi} A_{eff} k_{2,\theta} \frac{f_y}{\gamma_{M,fi}}} \quad \text{for slender sections.} \quad (24)$$

The interaction factors k_{yz} and k_{zy} are determined using the following equations in accordance with prEN 1993-1-1 [20]:

$$k_{yz} = k_{zz} \quad (25)$$

$$k_{zy} = 0.8k_{yy}. \quad (26)$$

In eqs. (19)–(20) and eqs. (21)–(22), D_y and D_z are stainless steel grade–dependent auxiliary coefficients used in the determination of the interaction factors. Following the approach described in Boissonnade et al. [37], these coefficients were determined through the calibration of the proposed interaction factors (i.e. k_{yy} and k_{zz}) against those obtained from the GMNIA of the stainless steel beam-column finite element models. The interaction factors from the GMNIA of the finite element models k_{FE} were determined considering a re-arrangement of the interaction formulae given by eq. (15)–(16) and eq. (17)–(18) as:

$$k_{FE} = (1 - n) \frac{M_{fi,\theta,Rd}}{M_{fi,Ed}} \quad \text{where} \quad n = \frac{N_{fi,Ed}}{N_{b,fi,\theta,Rd}}. \quad (27)$$

In eq. (27), $N_{b,fi,\theta,Rd}$ is the flexural buckling resistance and $M_{fi,\theta,Rd}$ is the bending moment resistance of the beam-column about the axis of applied bending $M_{fi,Ed}$. The calibration of k_{yy} and k_{zz} of the new proposals (i.e. $k_{yy,prop}$ and $k_{zz,prop}$) against the k_{FE} values determined through the GMNIA of austenitic, duplex and ferritic stainless steel beam-columns with a European HEM 100 cross-section is shown in Figs. 16–21. Note that in Figs. 16–21, the flexural buckling resistances of the beam-columns $N_{b,fi,\theta,Rd}$ obtained from GMNIA are used. The calibrated values of the auxiliary coefficients D_y and D_z are provided in Table 4. Note that in eqs. (19)–(22), C_{my} and C_{mz} are the equivalent uniform moment factors defined in prEN 1993-1-1 [20], which are equal to unity for beam-columns under uniform bending moment. Additionally, it should also be noted that, while the use of the effective width method established in [16] is recommended for the determination of the effective cross-section properties (i.e. A_{eff} , $W_{y,eff}$ and $W_{z,eff}$) of stainless steel members under major axis bending plus axial compression, the use of the plastic effective width method provided in [38, 39] is recommended for stainless steel beam-columns under minor axis bending and axial compression to achieve more accurate ultimate strength predictions, as verified by Xing et al. [36, 39].

4.2. Assessment of accuracy and reliability of new proposals

In this subsection, the accuracy of the new stainless steel beam-column fire design proposals is assessed against the numerical data from the nonlinear finite element modelling, considering

the broad range of cases summarised in Table 3. Figs. 10–15 show the accuracy of the new proposals against the GMNIA results for I-section beam-columns equivalent to a European HEM 200 profile for the austenitic stainless steel members, an HEB 300 section for the duplex stainless steel members and an HEAA 180 section for the ferritic stainless steel members; the level of the accuracy of the current EN 1993-1-2 [19] beam-column design rules is also illustrated in the figures. As can be seen from Figs. 10–15, the new proposals lead to significantly more accurate and safe-sided ultimate strength predictions for stainless steel beam-columns in fire relative to the current EN 1993-1-2 [19] beam-column design rules.

The accuracy of the new proposals is also assessed by comparing the numerical failure loads N_u to the predicted resistances $N_{u,pred}$ for different radial angles ϕ , considering the broad range of parameters provided in Table 3. As shown in Fig. 8, if the ratio of N_u to $N_{u,pred}$ is greater than or equal to unity (i.e. $N_u/N_{u,pred} \geq 1.0$), the predicted design resistance $N_{u,pred}$ is on the safe side. The predicted resistances $N_{u,pred}$ are obtained by assuming that the beam-columns are subjected to proportional loading in accordance with the procedure reported in [40–42]. The accuracy of the new proposals is assessed in Fig. 22 for the stainless steel beam-columns under major axis bending plus axial compression and in Fig. 23 for the stainless steel beam-columns under minor axis bending plus axial compression; an assessment of the EN 1993-1-2 [19] beam-column design rules is also provided for comparison in Figs. 22–23. As can be seen from the figures, the new proposals lead to significantly enhanced accuracy with a lower level of scatter relative to the existing EN 1993-1-2 [19] rules for the design of stainless steel I-section beam-columns in fire.

A statistical appraisal of the accuracy of the new proposals is provided in Table 5. In the table, ε_{av} , ε_{COV} , ε_{max} and ε_{min} are the mean value, coefficient of variation (COV), maximum value and minimum value, respectively, of the ratios of the ultimate resistances obtained from the finite element modelling to the corresponding predictions from the design methods i.e. $\varepsilon = N_u/N_{u,pred}$. As can be seen from Table 5, the new proposals lead to accurate and safe-sided ultimate strength predictions for all the considered stainless steel beam-columns with low ε_{COV} values, while the current EN 1993-1-2 [19] design rules generally result in unsafe strength predictions with high ε_{COV} values, thus demonstrating the increased level of accuracy achieved through the new design proposals.

Finally, in Table 6, the reliability of the new proposals is assessed on the basis of the three fire design reliability criteria put forward by Kruppa [1]. The first criterion of Kruppa [1] states that the ultimate resistances predicted by a design method $N_{u,pred}$ should not exceed the numerical results obtained from nonlinear finite element modelling N_u by more than 15% (i.e. $\max(N_{u,pred}/N_u) \leq 1.15$); the second criterion of [1] states that less than 20% of the design predictions should be on the unsafe side (i.e. $\text{num}(N_{u,pred} > N_u)/\text{num}(N_u) \leq 20\%$); and the third criterion of [1] states that the average of the design predictions should be on the safe side (i.e. $\frac{1}{n} \sum [(N_{u,pred} - N_u)/N_u] \leq 0\%$, where n is the number of FE results). The reliability of the EN 1993-1-2 [19] beam-column design rules is also assessed in Table 6. Note that in the table, a number denoted by ‘*’ indicates the cases for which the reliability criteria are not satisfied. As can be seen from Table 6, the new beam-column design proposals satisfy all the reliability criteria of Kruppa [1], confirming their suitability for inclusion in the upcoming revision to EN 1993-1-2, while the current EN 1993-1-2

[19] beam-column design rules fail to satisfy the criteria in a high number of cases.

5. Conclusions

A new design method for stainless steel beam-columns in fire has been developed in this paper. Finite element models able to replicate the structural behaviour of stainless steel I-section beam-columns at elevated temperatures were created and validated against experimental data. Parametric studies were subsequently performed by carrying out the Geometrically and Materially Nonlinear Analyses with Imperfections (GMNIA) using the validated finite element models, in which a wide range of stainless steel grades, cross-section geometries, elevated temperature levels and slendernesses were considered. Using the obtained GMNIA results, the shortcomings of the current EN 1993-1-2 [19] were revealed, highlighting the need for the development of improved fire design rules for stainless steel beam-columns. New beam-column design rules were derived, adopting the format used in the beam-column design equations of the upcoming European standard for room temperature structural steel design prEN1993-1-1 [20] to achieve consistency between room temperature and fire design rules for beam-columns. The accuracy of the proposed beam-column design rules was assessed against the GMNIA results. It was shown that the new beam-column design rules provided more consistent and safe-sided resistance predictions than the existing EN 1993-1-2 [19] design rules, and satisfied the fire design reliability criteria of Kruppa [1] in all cases, confirming their suitability for inclusion in the upcoming revision to EN 1993-1-2. In this paper, the behaviour of stainless steel beam columns subjected to combined uniform bending and compression has been investigated. Future research will focus on the assessment of the proposed fire design rules for stainless steel beam-columns under non-uniform bending plus axial compression.

References

- [1] J. Kruppa, Eurocodes–Fire parts: Proposal for a methodology to check the accuracy of assessment methods, CEN TC 250, Horizontal Group Fire, Document no: 99/130, 1999.
- [2] L. Gardner, Stability and design of stainless steel structures – review and outlook, *Thin-Walled Structures* 141 (2019) 208–216.
- [3] B. Uppfeldt, T. Ala-Outinen, M. Veljkovic, A design model for stainless steel box columns in fire, *Journal of Constructional Steel Research* 64 (11) (2008) 1294–1301.
- [4] E. C.-Y. To, B. Young, Performance of cold-formed stainless steel tubular columns at elevated temperatures, *Engineering Structures* 30 (7) (2008) 2012–2021.
- [5] N. Lopes, P. Vila-Real, L. da Silva, J.-M. Franssen, Axially loaded stainless steel columns in case of fire, *Journal of Structural Fire Engineering* 1 (1) (2010) 43–60.
- [6] N. Tondini, B. Rossi, J.-M. Franssen, Experimental investigation on ferritic stainless steel columns in fire, *Fire Safety Journal* 62 (2013) 238–248.
- [7] S. Fan, X. Ding, W. Sun, L. Zhang, M. Liu, Experimental investigation on fire resistance of stainless steel columns with square hollow section, *Thin-Walled Structures* 98 (2016) 196–211.
- [8] R. Ding, S. Fan, G. Chen, C. Li, E. Du, C. Liu, Fire resistance design method for restrained stainless steel H-section columns under axial compression, *Fire Safety Journal* 108 (2019) 102837.
- [9] A. Mohammed, S. Afshan, Numerical modelling and fire design of stainless steel hollow section columns, *Thin-Walled Structures* 144 (2019) 106243.
- [10] K. Ng, L. Gardner, Buckling of stainless steel columns and beams in fire, *Engineering Structures* 29 (5) (2007) 717–730.

- [11] P. Vila-Real, N. Lopes, L. S. da Silva, J.-M. Franssen, Lateral-torsional buckling of stainless steel I-beams in case of fire, *Journal of Constructional Steel Research* 64 (11) (2008) 1302–1309.
- [12] N. Lopes, P. Vila-Real, L. S. da Silva, J.-M. Franssen, Numerical analysis of stainless steel beam-columns in case of fire, *Fire Safety Journal* 50 (2012) 35–50.
- [13] N. Lopes, M. Manuel, A. R. Sousa, P. Vila-Real, Parametric study on austenitic stainless steel beam-columns with hollow sections under fire, *Journal of Constructional Steel Research* 152 (2019) 274–283.
- [14] S. Fan, M. Liu, W. Sun, Y. Guo, Y. L. Han, Experimental investigation of eccentrically compressed stainless steel columns with constraints in fire, *Fire Safety Journal* 99 (2018) 49–62.
- [15] Z. Xing, O. Zhao, M. Kucukler, L. Gardner, Fire testing of stainless steel I-section beam-columns, *Thin-Walled Structures*, Submitted for publication.
- [16] Z. Xing, M. Kucukler, L. Gardner, Local buckling of stainless steel plates in fire, *Thin-Walled Structures* 148 (2020) 106570.
- [17] M. Kucukler, Z. Xing, L. Gardner, Behaviour and design of stainless steel I-section columns in fire, *Journal of Constructional Steel Research* 165 (2020) 105890.
- [18] M. Kucukler, Z. Xing, L. Gardner, Lateral-torsional buckling assessment of stainless steel beams in fire, *Journal of Constructional Steel Research*, Submitted for publication (2020).
- [19] EN 1993-1-2, Eurocode 3 Design of steel structures-Part 1-2: General rules – Structural fire design, European Committee for Standardization (CEN), Brussels, 2005.
- [20] prEN 1993-1-1, Eurocode 3 Design of steel structures-Part 1-1: General rules and rules for buildings, European Committee for Standardization (CEN), Brussels, 2020.
- [21] Abaqus v.6.14 Reference Manual, Simulia, Dassault Systemes, 2014.
- [22] M. Kucukler, L. Gardner, Design of laterally restrained web-tapered steel structures through a stiffness reduction method, *Journal of Constructional Steel Research* 141 (2018) 63–76.
- [23] M. Kucukler, L. Gardner, Design of web-tapered steel beams against lateral-torsional buckling through a stiffness reduction method, *Engineering Structures* 190 (2019) 246–261.
- [24] M. Kucukler, Compressive resistance of high-strength and normal-strength steel CHS members at elevated temperatures, *Thin-Walled Structures* 152 (2020) 106753.
- [25] M. Kucukler, Lateral instability of steel beams in fire: Behaviour, numerical modelling and design, *Journal of Constructional Steel Research* 170 (2020) 106095.
- [26] W. Ramberg, W. R. Osgood, Description of stress-strain curves by three parameters, Technical note no. 902, National Advisory Committee on Aeronautics (NACA), 1943.
- [27] L. Gardner, X. Yun, Description of stress-strain curves for cold-formed steels, *Construction and Building Materials* 189 (2018) 527–538.
- [28] I. Arrayago, E. Real, L. Gardner, Description of stress-strain curves for stainless steel alloys, *Materials & Design* 87 (2015) 540–552.
- [29] Y. Liang, T. Manninen, O. Zhao, F. Walport, L. Gardner, Elevated temperature material properties of a new high-chromium austenitic stainless steel, *Journal of Constructional Steel Research* 152 (2019) 261–273.
- [30] S. Afshan, O. Zhao, L. Gardner, Standardised material properties for numerical parametric studies of stainless steel structures and buckling curves for tubular columns, *Journal of Constructional Steel Research* 152 (2019) 2–11.
- [31] Design manual for structural stainless steel, Fourth Edition, Steel Construction Institute (SCI), 2017.
- [32] H. Yuan, Y. Wang, Y. Shi, L. Gardner, Residual stress distributions in welded stainless steel sections, *Thin-Walled Structures* 79 (2014) 38–51.
- [33] M. Jandera, L. Gardner, J. Machacek, Residual stresses in cold-rolled stainless steel hollow sections, *Journal of Constructional Steel Research* 64 (11) (2008) 1255–1263.
- [34] EN 1993-1-4, Eurocode 3 Design of steel structures-Part 1-4: General rules – Supplementary rules for stainless steel, European Committee for Standardization (CEN), Brussels, 2005.
- [35] C. Couto, A. Sanzel, P. Vila-Real, N. Lopes, B. Zhao, Beam-columns with thin wall cross-sections in case of fire, 9th International Conference Structures in Fire, 2016.
- [36] Z. Xing, M. Kucukler, L. Gardner, Local buckling of stainless steel I-sections in fire: finite element modelling and design, *Thin-Walled Structures*, Submitted for publication (2020).

- [37] N. Boissonnade, R. Greiner, J.-P. Jaspart, J. Lindner, Rules for member stability in en 1993-1-1: Background documentation and design guidelines, ECCS European Convention for Constructional Steelwork, 2006.
- [38] M. R. Bambach, K. J. Rasmussen, Effective widths of unstiffened elements with stress gradient, *Journal of Structural Engineering*, ASCE 130 (10) (2004) 1611–1619.
- [39] Z. Xing, O. Zhao, M. Kucukler, L. Gardner, Testing and design of slender stainless steel I-sections in minor axis bending in fire, *Thin-Walled Structures*; Submitted for publication.
- [40] O. Zhao, B. Rossi, L. Gardner, B. Young, Behaviour of structural stainless steel cross-sections under combined loading – part II: Numerical modelling and design approach, *Engineering Structures* 89 (2015) 247–259.
- [41] L. Yang, M. Zhao, L. Gardner, K. Ning, J. Wang, Member stability of stainless steel welded I-section beam-columns, *Journal of Constructional Steel Research* 155 (2019) 33–45.
- [42] Y. Bu, L. Gardner, Laser-welded stainless steel I-section beam-columns: Testing, simulation and design, *Engineering Structures* 179 (2019) 23–36.
- [43] C. Buchanan, O. Zhao, E. Real, L. Gardner, Cold-formed stainless steel CHS beam-columns–Testing, simulation and design, *Engineering Structures* 213 (2020) 110270.
- [44] O. Zhao, L. Gardner, B. Young, Experimental study of ferritic stainless steel tubular beam-column members subjected to unequal end moments, *Journal of Structural Engineering*, ASCE 142 (11) (2016) 04016091.
- [45] O. Zhao, L. Gardner, B. Young, Finite element modelling and design of stainless steel SHS and RHS beam-columns under moment gradients, *Thin-Walled Structures* 134 (2019) 220–232.
- [46] O. Zhao, L. Gardner, B. Young, Behaviour and design of stainless steel SHS and RHS beam-columns, *Thin-Walled Structures* 106 (2016) 330–345.

6. Figures

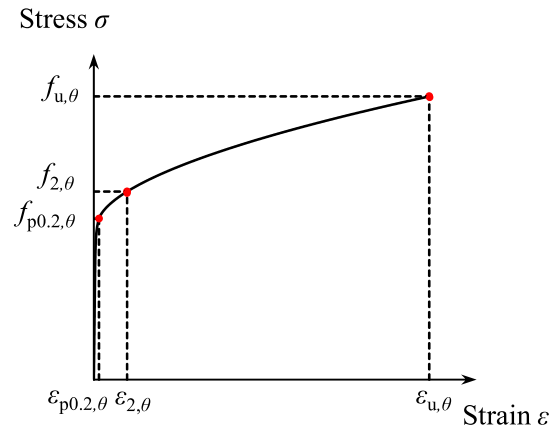
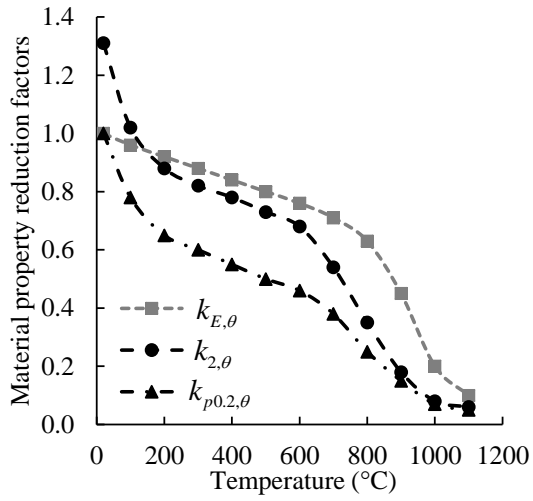


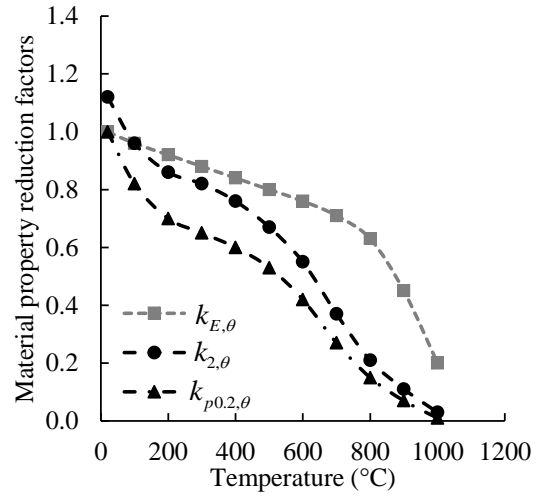
Figure 1: Two-stage elevated temperature Ramberg-Osgood material model adopted in FE models



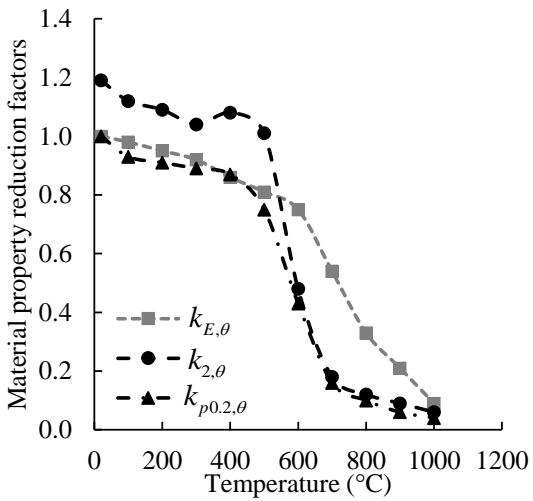
Figure 2: Experimental and numerical failure modes for specimen BC-Z10-0.4 [15]



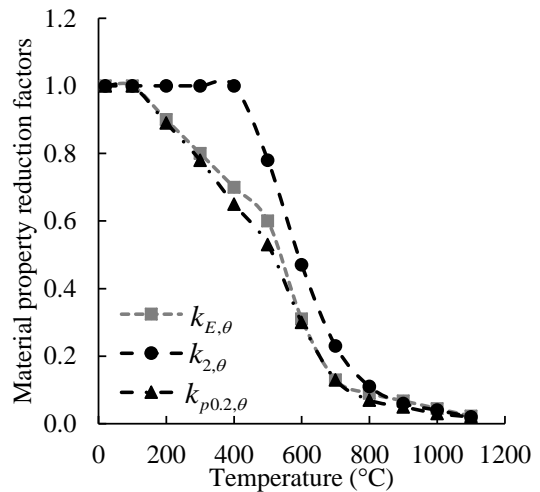
(a) Austenitic stainless steel



(b) Duplex stainless steel



(c) Ferritic stainless steel



(d) Carbon steel

Figure 3: Strength ($k_{2,\theta}$, $k_{p0.2,\theta}$) and stiffness ($k_{E,\theta}$) reduction factors for different stainless steel grades considered in this paper and carbon steel at elevated temperatures

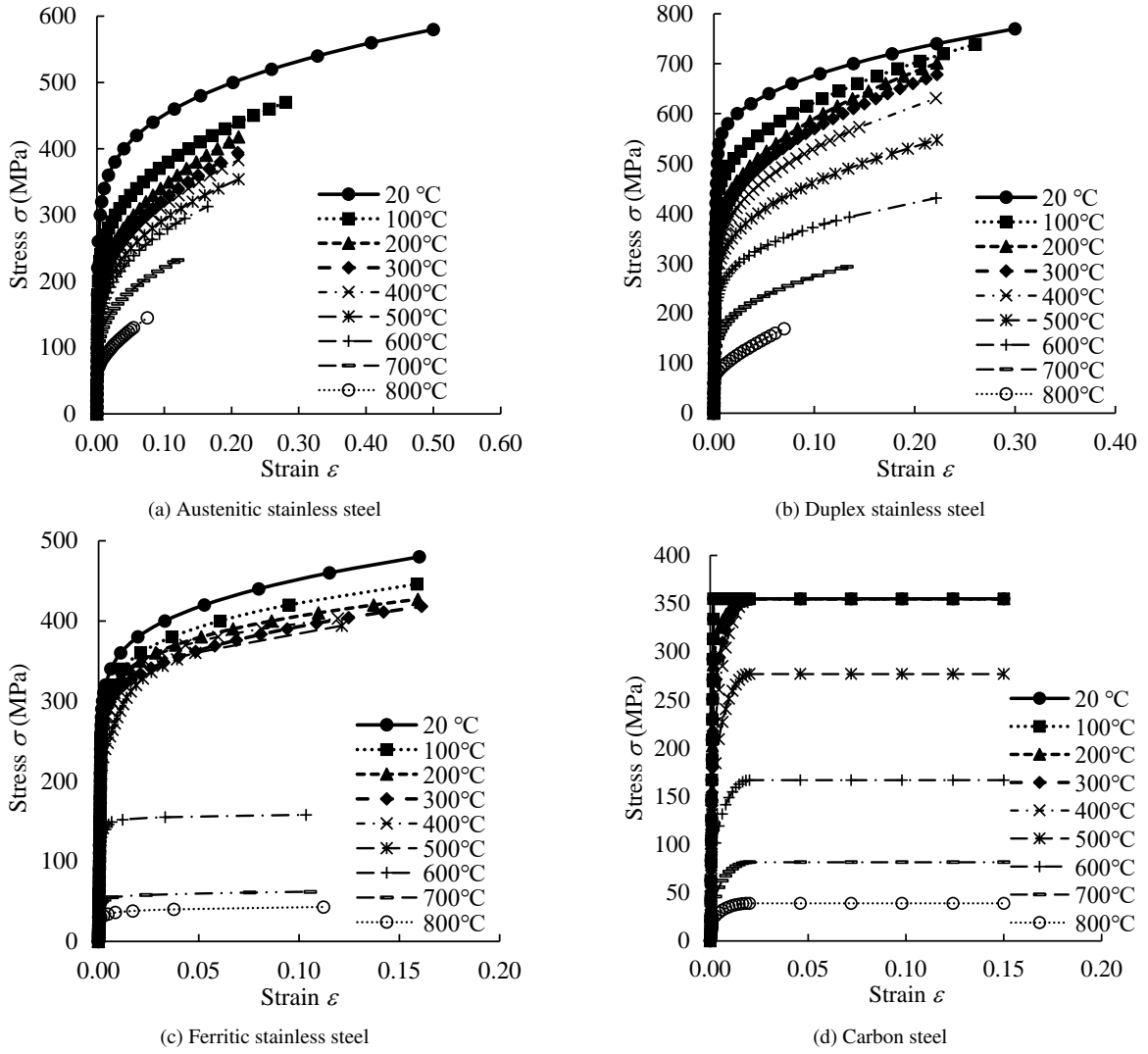
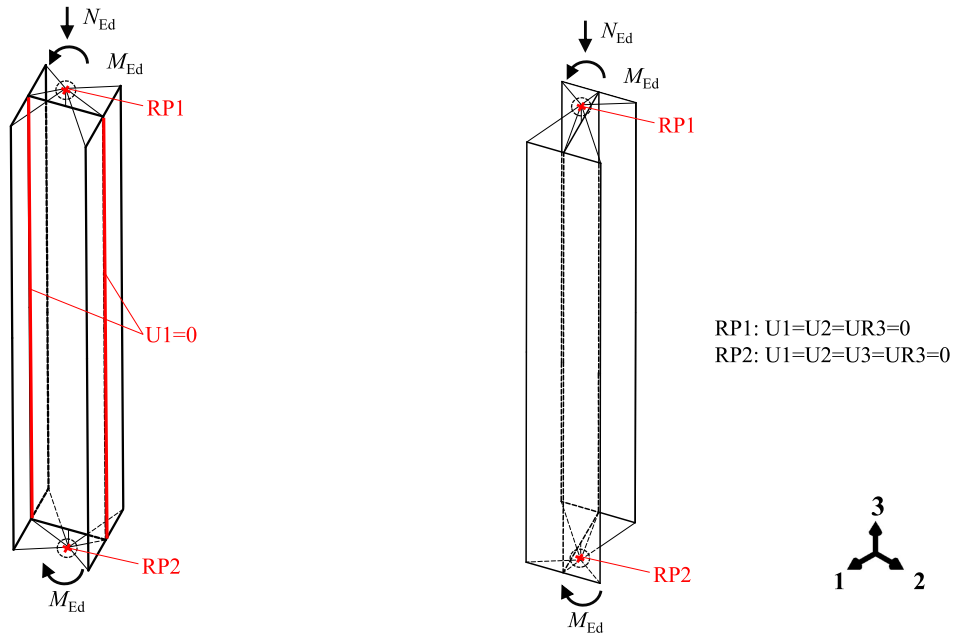
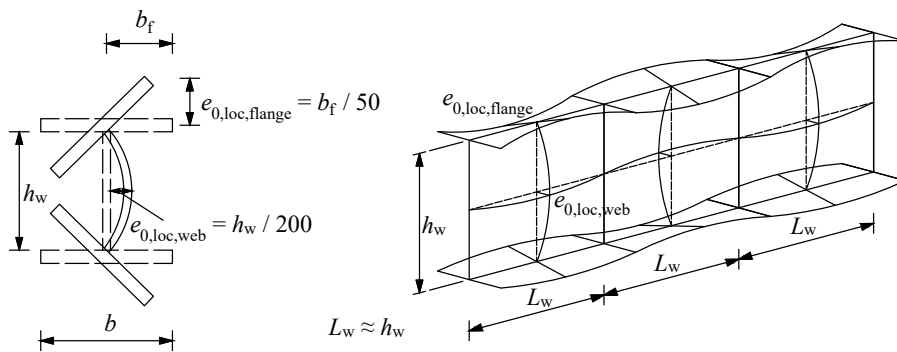


Figure 4: Stress-strain response of different stainless steel grades and carbon steel at elevated temperatures

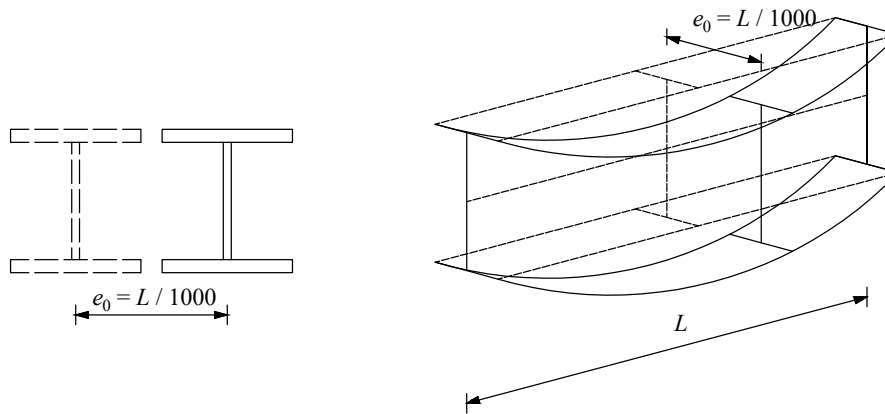


(a) Beam-columns under major axis bending plus axial compression (b) Beam-columns under minor axis bending plus axial compression

Figure 5: Boundary conditions applied to beam-column finite element models



(a) Local imperfection



(b) Global imperfection

Figure 6: Local and global imperfections applied to finite element models

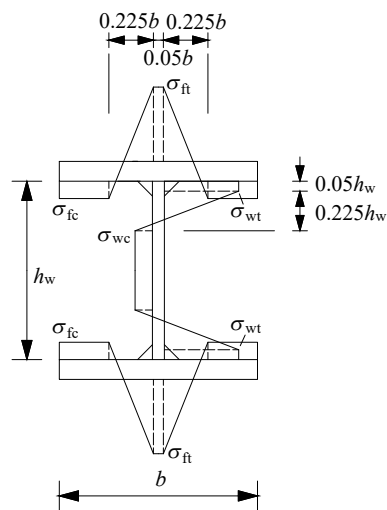


Figure 7: Residual stress patterns applied to finite element models

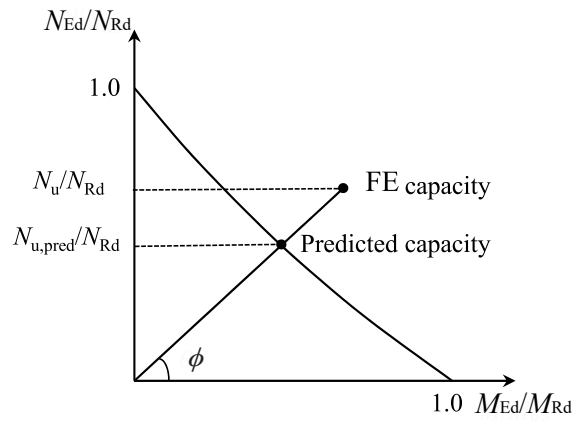
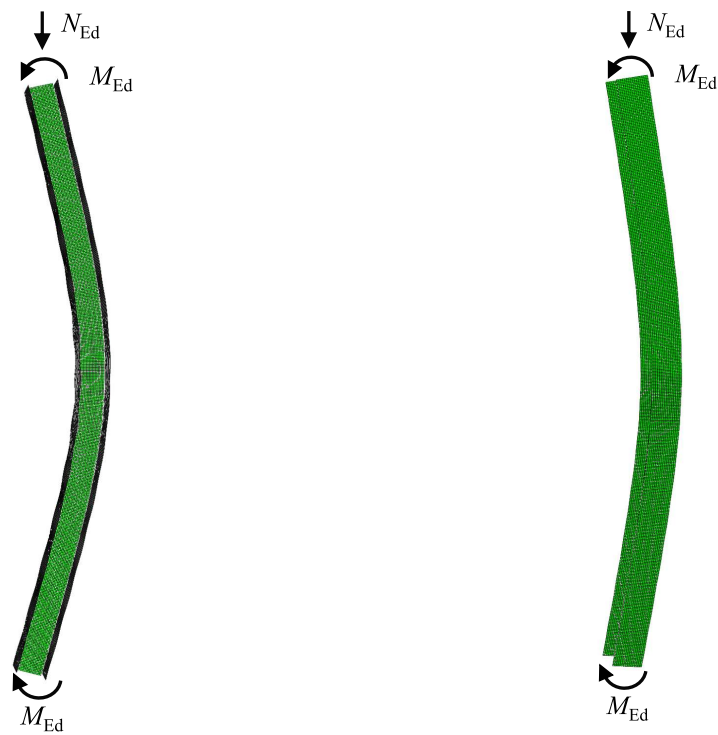


Figure 8: Definition of radial angle ϕ on axial load-moment interaction curve



(a) Beam-columns under major axis bending plus axial compression (b) Beam-columns under minor axis bending plus axial compression

Figure 9: Typical failure modes of stainless steel beam-columns under different loading conditions

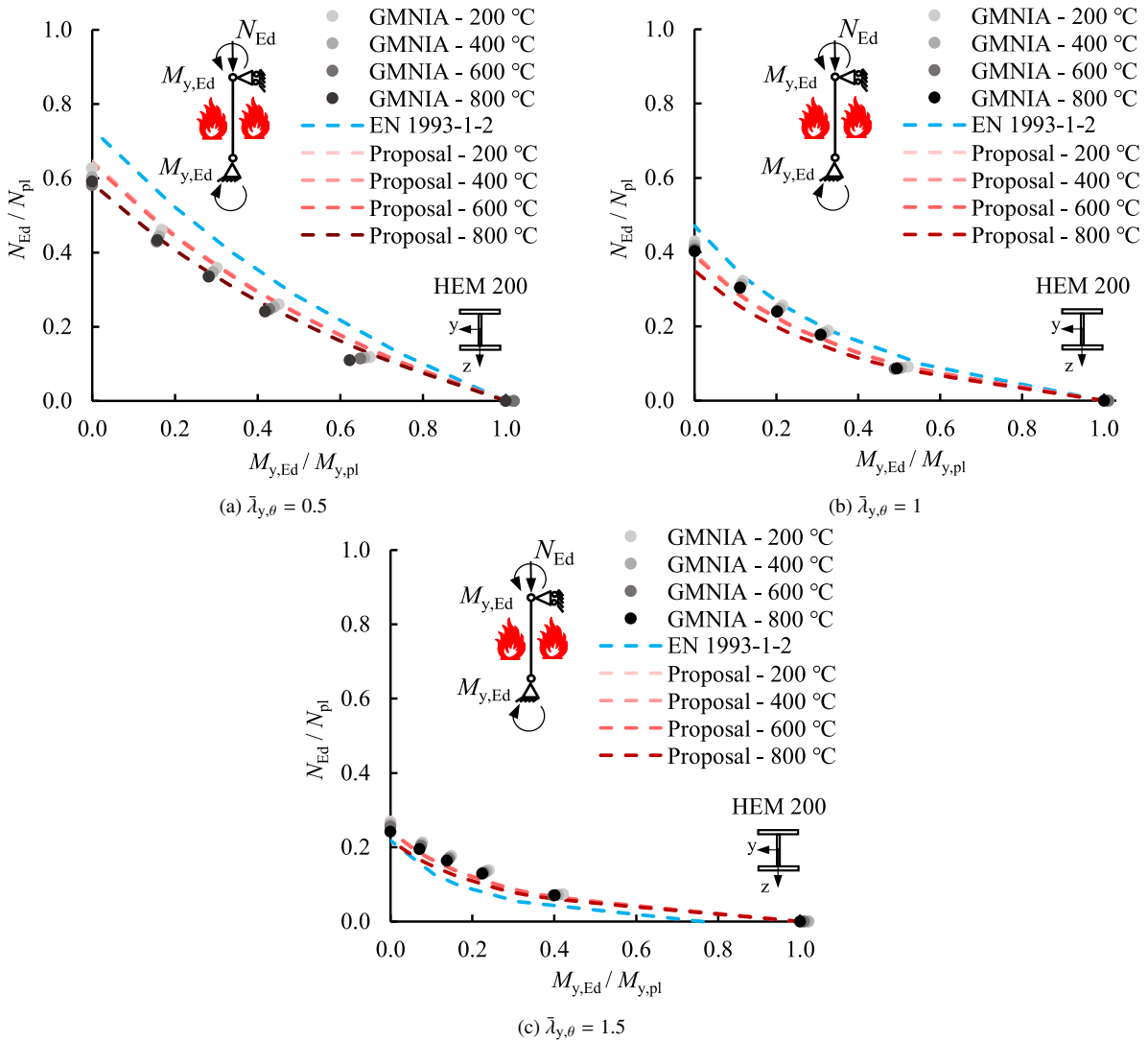


Figure 10: Assessment of EN 1993-1-2 [19] and new proposals for austenitic stainless steel beam-columns under major axis bending plus axial compression

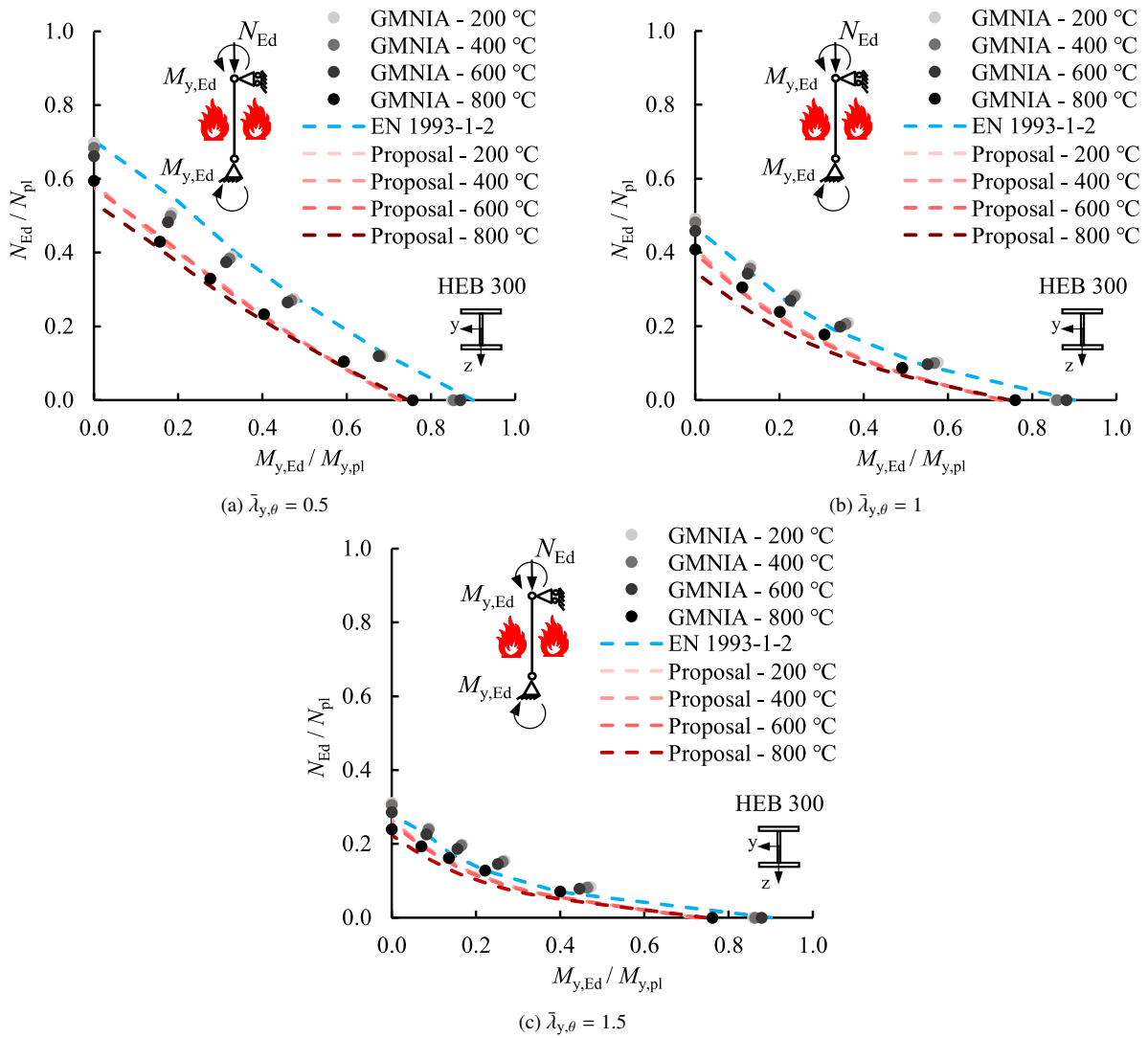


Figure 11: Assessment of EN 1993-1-2 [19] and new proposals for duplex stainless steel beam-columns under major axis bending plus axial compression

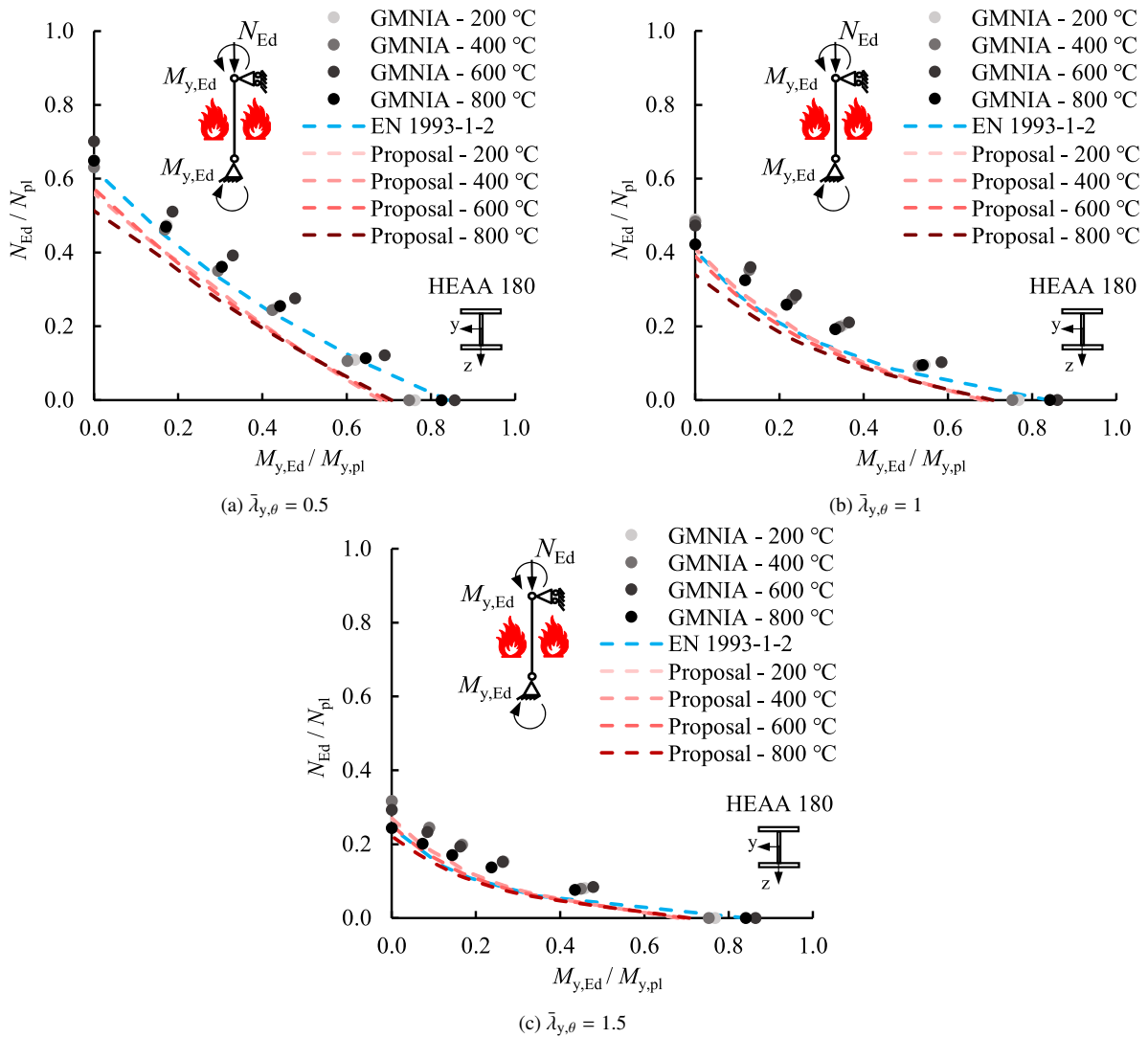


Figure 12: Assessment of EN 1993-1-2 [19] and new proposals for ferritic stainless steel beam-columns under major axis bending plus axial compression

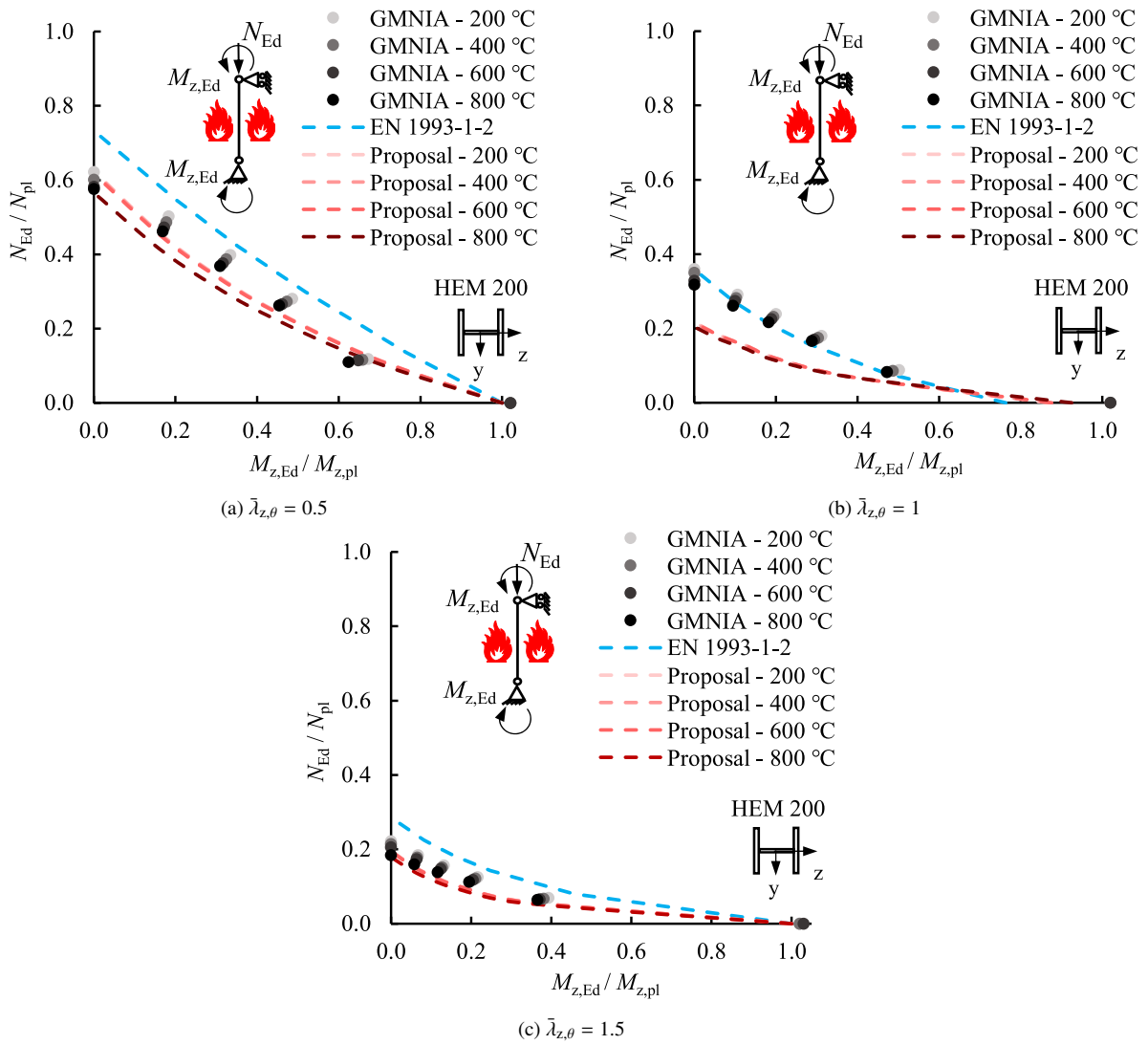


Figure 13: Assessment of EN 1993-1-2 [19] and new proposals for austenitic stainless steel beam-columns under minor axis bending plus axial compression

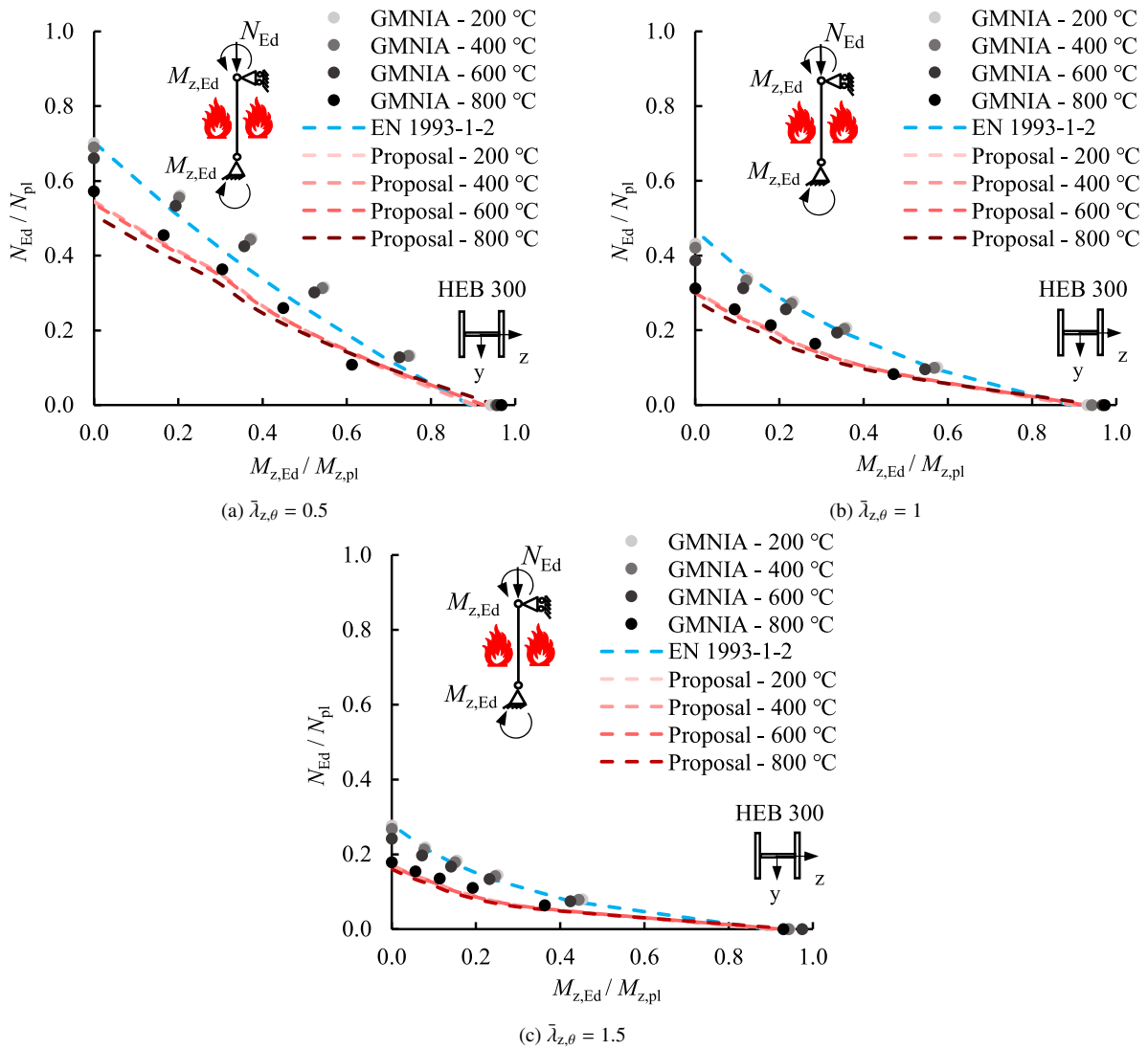


Figure 14: Assessment of EN 1993-1-2 [19] and new proposals for duplex stainless steel beam-columns under minor axis bending plus axial compression

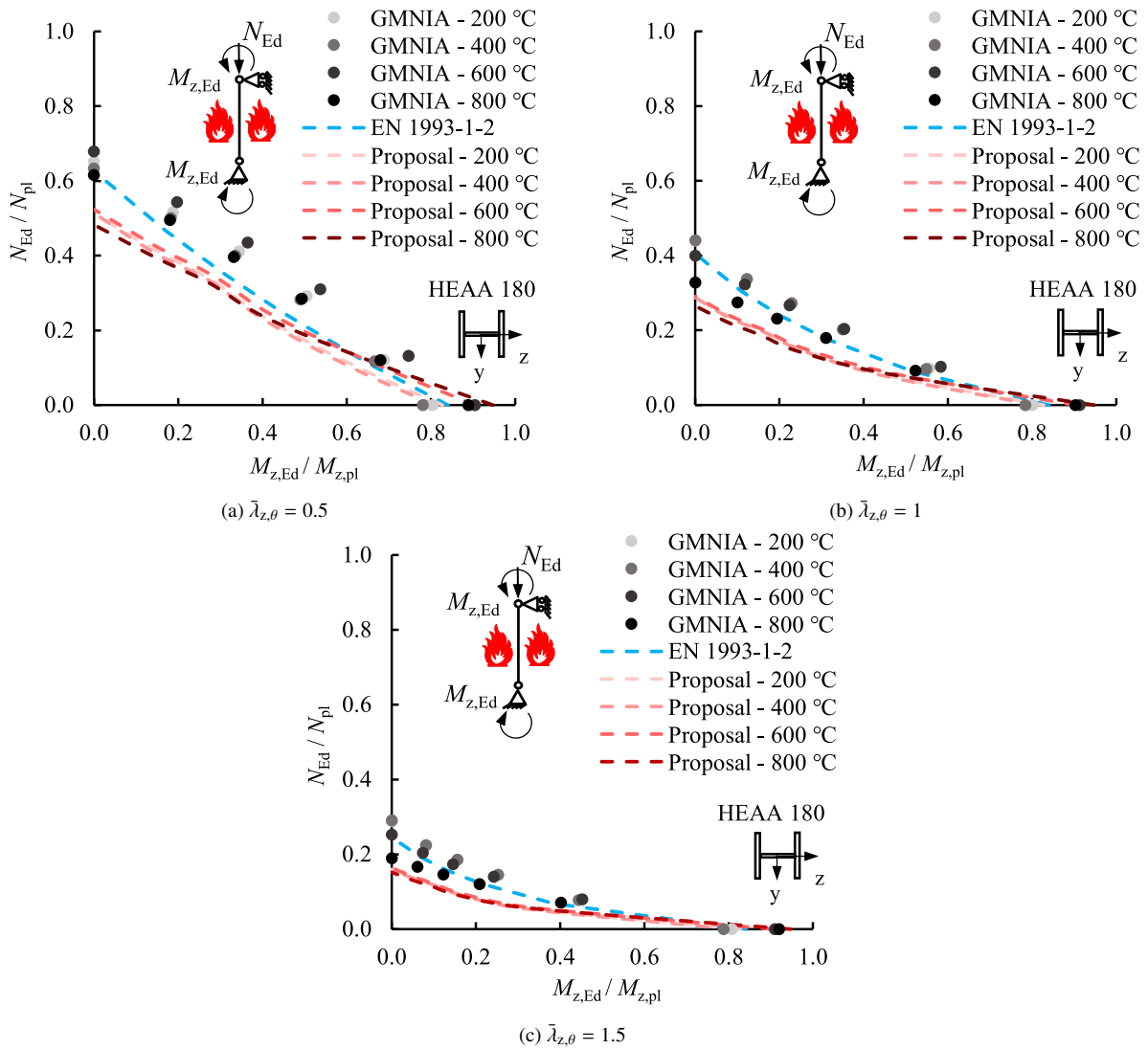


Figure 15: Assessment of EN 1993-1-2 [19] and new proposals for ferritic stainless steel beam-columns under minor axis bending plus axial compression

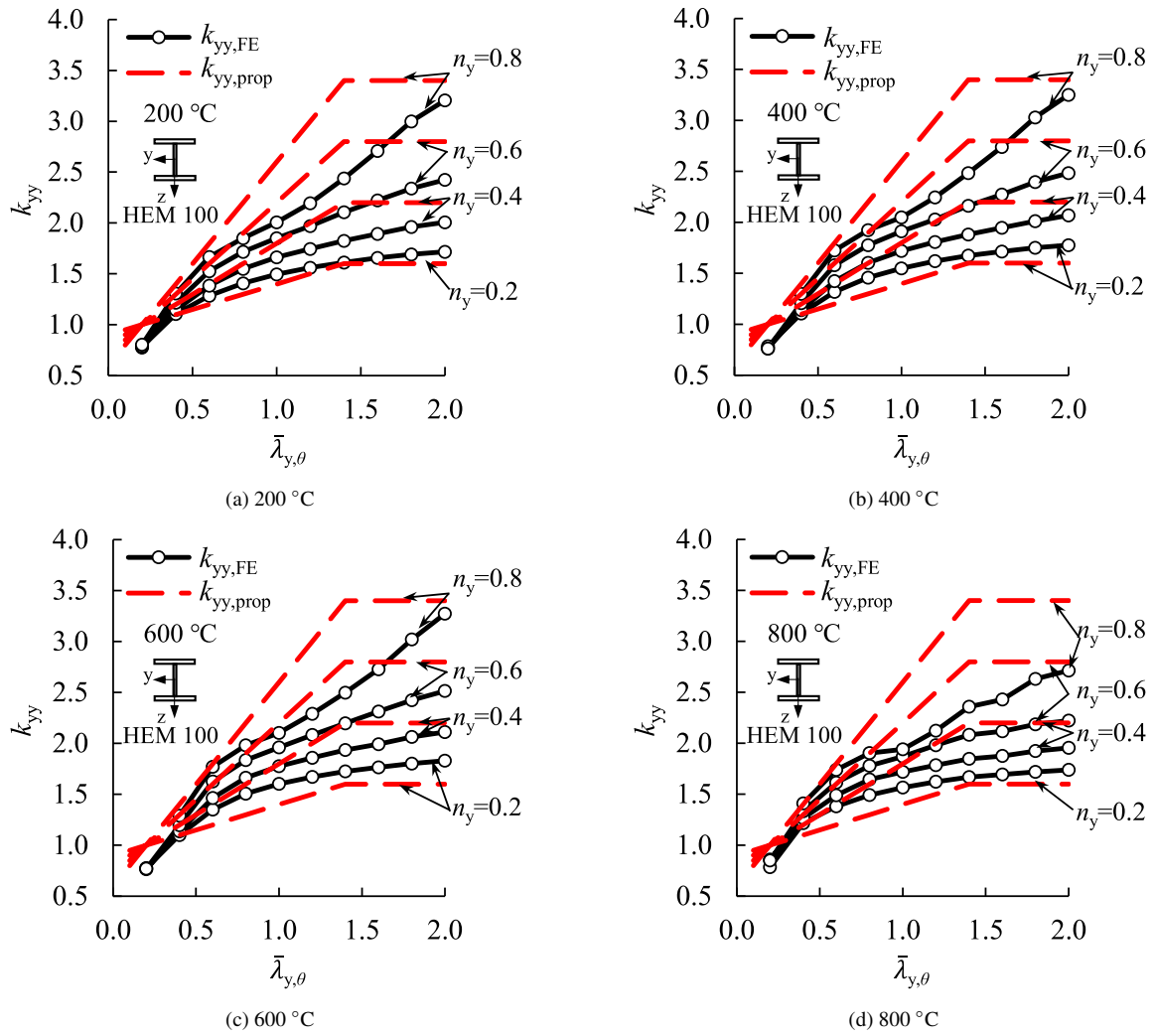


Figure 16: Calibration of interaction factors k_{yy} for austenitic stainless steel beam-columns in fire

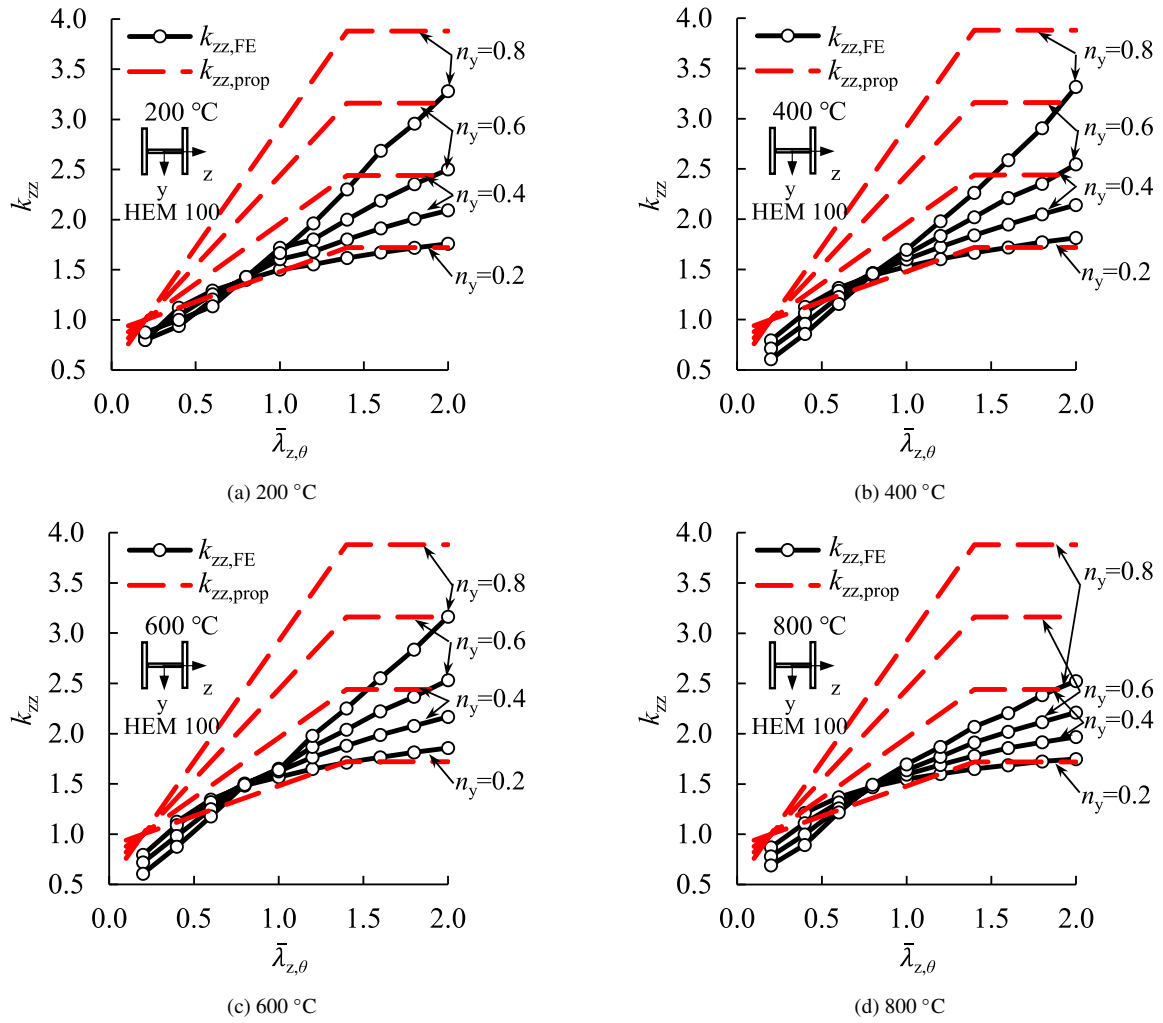


Figure 17: Calibration of interaction factors k_{zz} for austenitic stainless steel beam-columns in fire

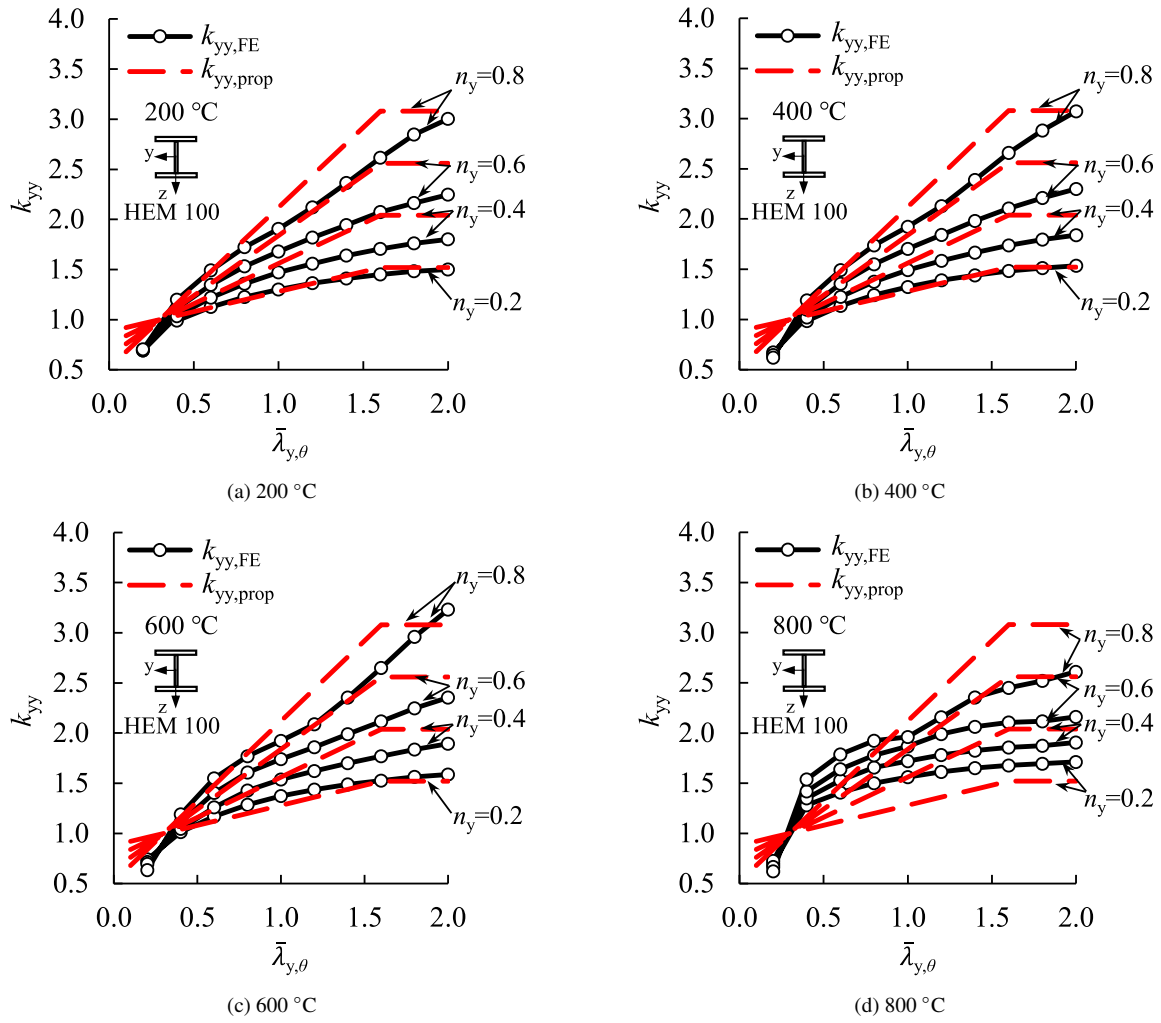


Figure 18: Calibration of interaction factors k_{yy} for duplex stainless steel beam-columns in fire

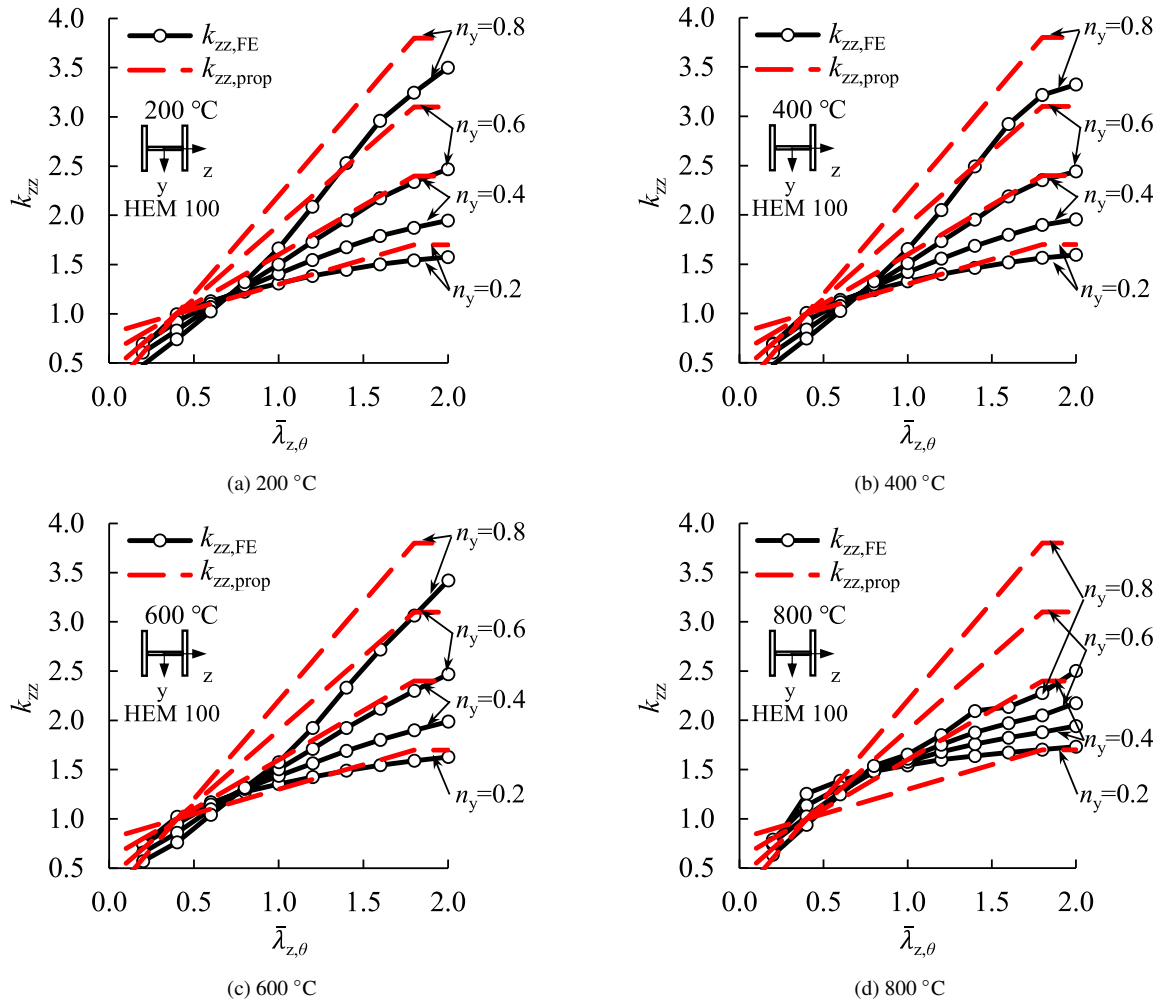


Figure 19: Calibration of interaction factors k_{zz} for duplex stainless steel beam-columns in fire

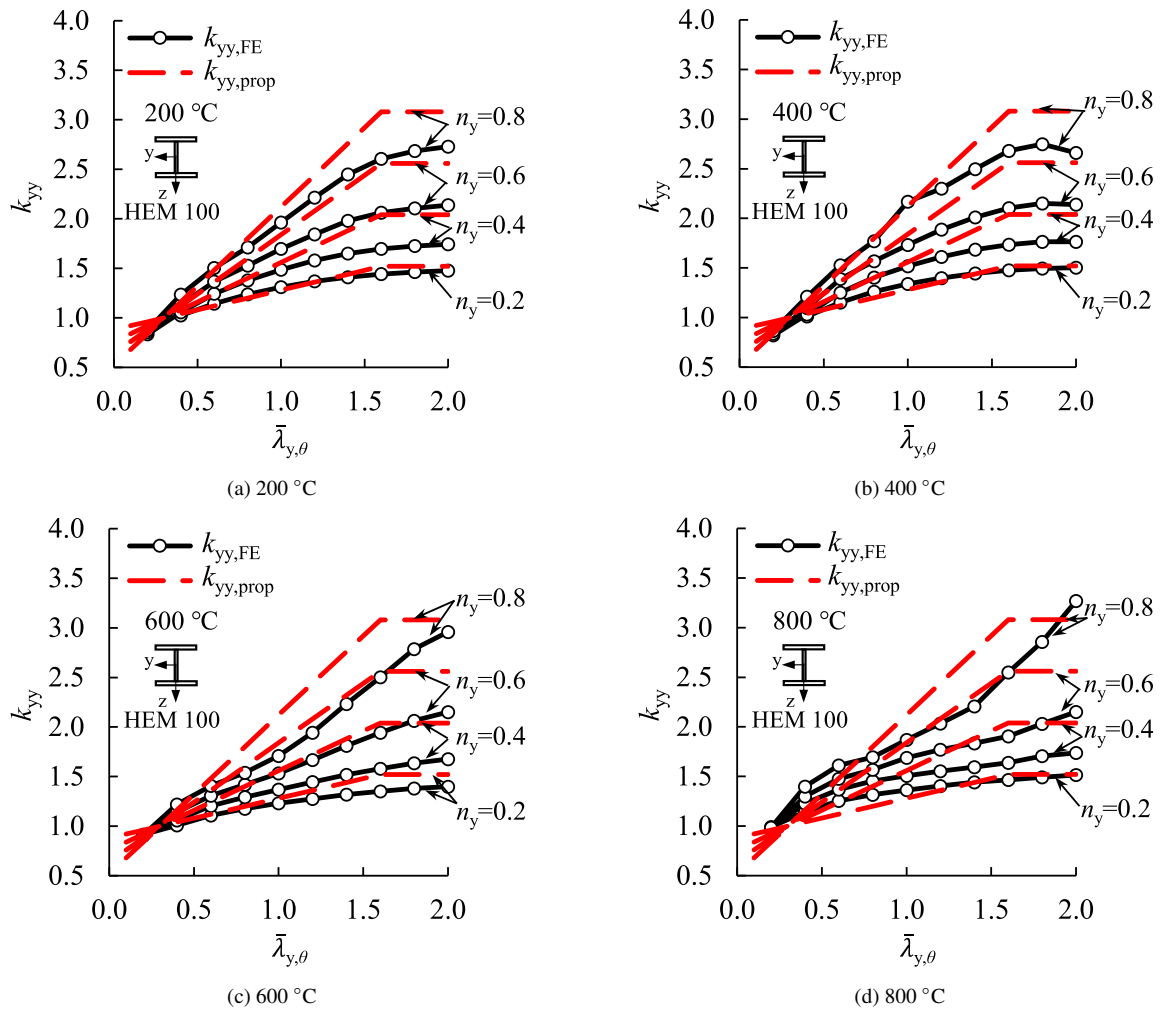


Figure 20: Calibration of interaction factors k_{yy} for ferritic stainless steel beam-columns in fire

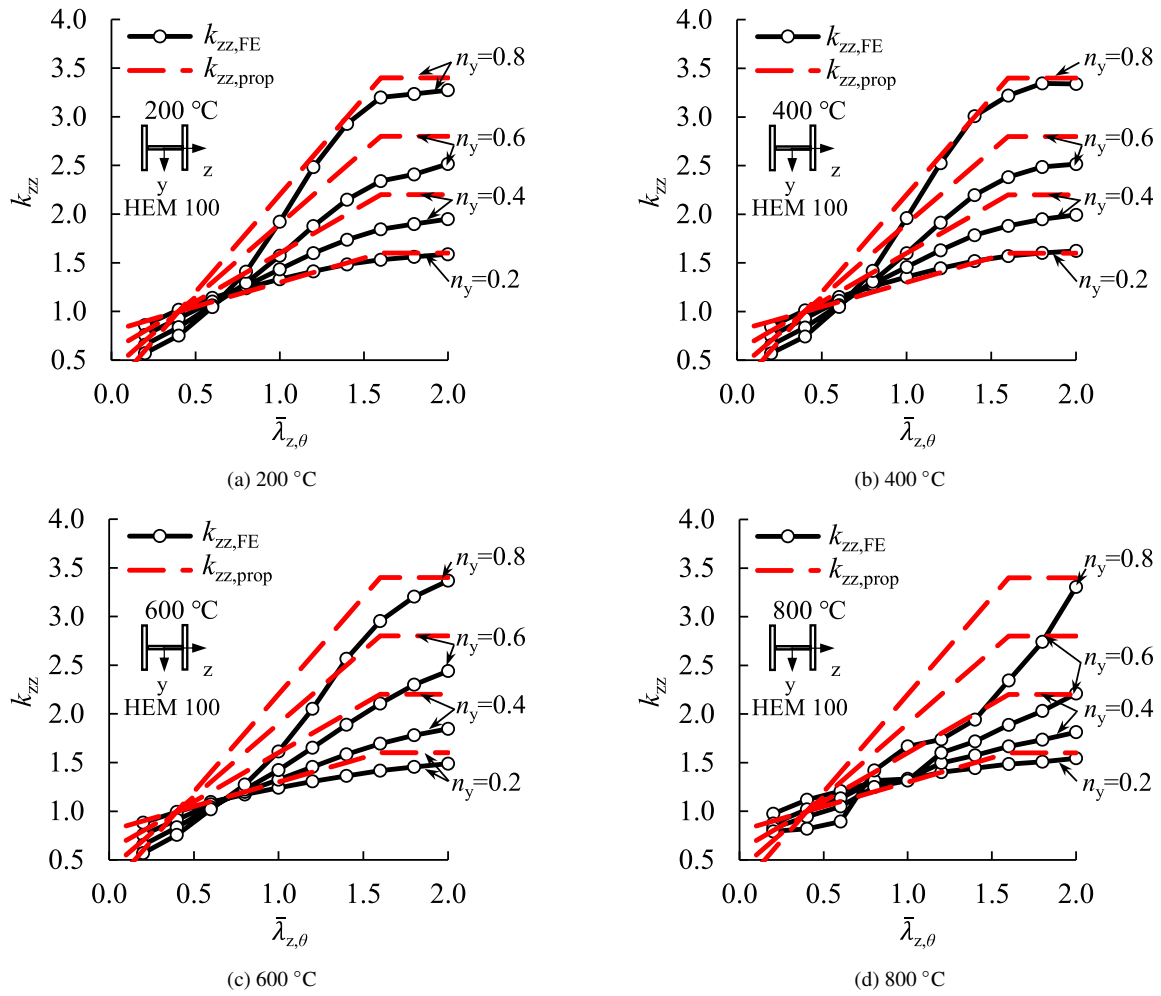


Figure 21: Calibration of interaction factors k_{zz} for ferritic stainless steel beam-columns in fire

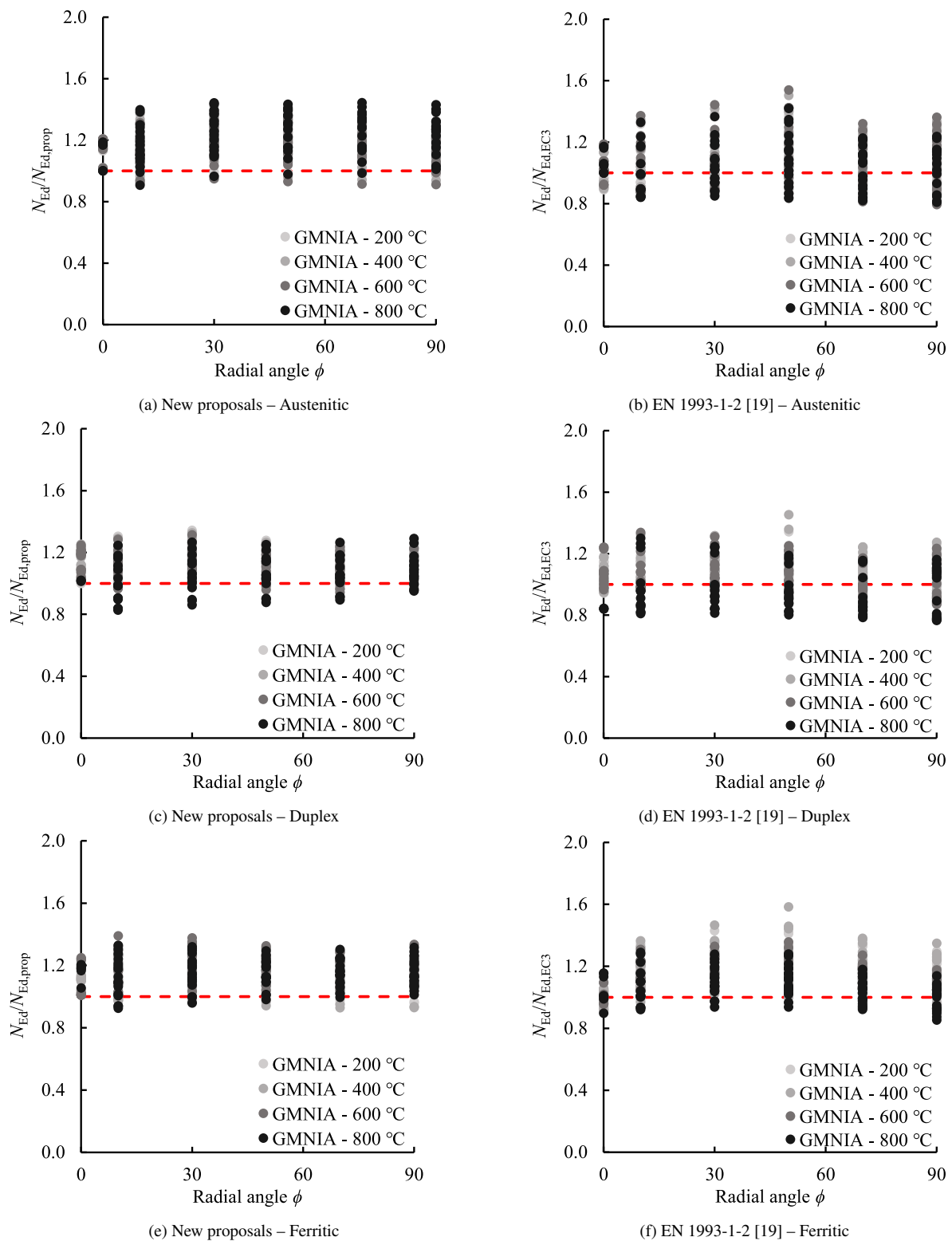


Figure 22: Comparison of accuracy of new proposals against FE results relative to EN 1993-1-2 [19] for stainless steel beam-columns under major axis bending plus axial compression in fire

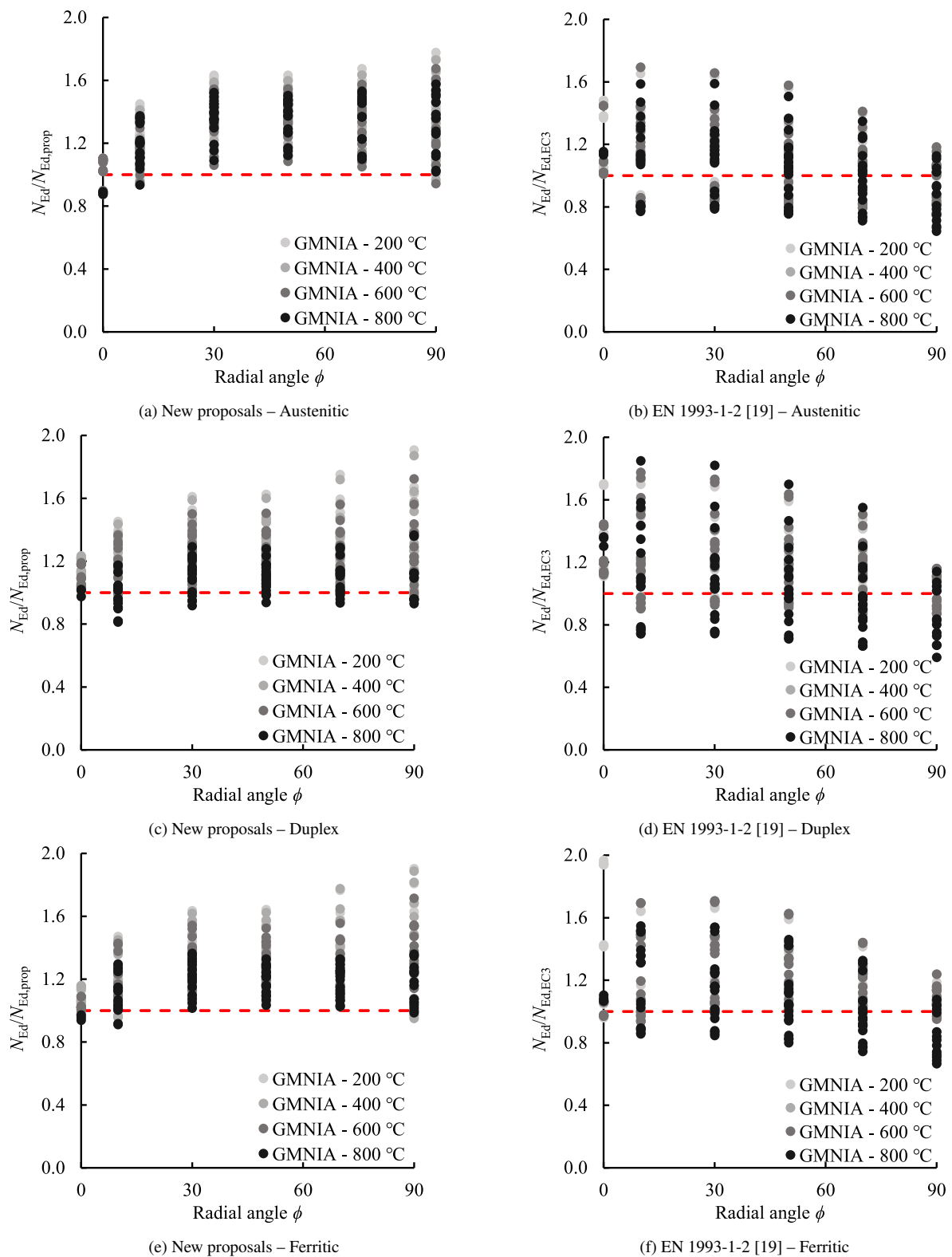


Figure 23: Comparison of accuracy of new proposals against FE results relative to EN 1993-1-2 [19] for stainless steel beam-columns under minor axis bending plus axial compression in fire

7. Tables

Table 1: Summary of room temperature material properties for austenitic, duplex and ferritic stainless steel grades used in this study

Material grade	E (GPa)	f_y (MPa)	f_u (MPa)	ε_u	$n_\theta (= n)$
Austenitic	200	280	580	0.50	9.1
Duplex	200	530	770	0.30	9.3
Ferritic	200	320	480	0.16	17.2

Table 2: Comparison of ultimate capacities of stainless steel beam-columns obtained from physical experiments reported in [15] and from FE analyses in this study

ID	Cross-section	θ_{cr} ($^{\circ}\text{C}$)	$N_{Ed,test}$ (kN)	$N_{Ed,FE}$ (kN)	$N_{Ed,FE}/N_{Ed,test}$
BC1-Z10-0.6	198×99×4.5×7	540	89	87	0.98
BC1-Z10-0.5	198×99×4.5×7	749	76	66	0.86
BC1-Z10-0.4	198×99×4.5×7	771	60	61	1.02
BC1-Z30-0.6	198×99×4.5×7	567	60	57	0.97
BC1-Z30-0.5	198×99×4.5×7	637	51	53	1.05
BC1-Z30-0.4	198×99×4.5×7	737	44	44	1.01
Average					0.98
COV					0.067

Table 3: Summary of parameters considered in numerical parametric studies carried out in this paper

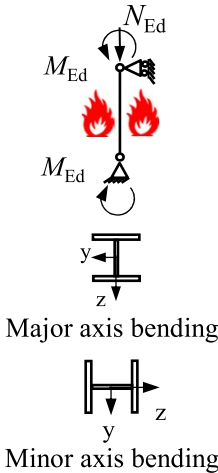
Loading condition	Stainless steel family	Cross-section	Temperature	Slenderness $\bar{\lambda}_\theta$	ϕ	
 <p>Major axis bending</p> <p>Minor axis bending</p>	Austenitic	HEM 200				
		HEAA 200				
		HEAA 300				
		IPE 100				
		IPE 200				
	Duplex	IPE 300				0°
		HEM 140	200°C	0.5	10°	
		HEB 300	400°C	1	30°	
		HEAA 200	600°C	1.5	50°	
		IPE 80	800°C		70°	
Ferritic	IPE 100				90°	
	IPE 100					
	IPE 180					
	HEM 200					
	HEAA 180					
		HEAA 300				
		IPE 100				
		IPE 180				
		IPE 300				

Table 4: Proposed values of auxiliary coefficients D_y and D_z

Coefficient	Austenitic	Duplex and Ferritic
$D_{1,y}$	2.5	2.0
$D_{2,y}$	0.2	0.3
$D_{3,y}$	1.4	1.6
$D_{1,z}$	3.0	2.5
$D_{2,z}$	0.2	0.4
$D_{3,z}$	1.4	1.8

Table 5: Assessment of new proposals against FE results relative to EN 1993-1-2 [19] for stainless steel beam-columns in fire

Loading condition	Design method	Grade	ε_{av}	ε_{COV}	ε_{max}	ε_{min}
Major axis bending plus axial compression	New proposal	Austenitic	1.19	0.10	1.44	0.91
		Duplex	1.12	0.09	1.34	0.83
		Ferritic	1.15	0.08	1.39	0.93
	EN 1993-1-2 [19]	Austenitic	1.05	0.136	1.54	0.79
		Duplex	1.06	0.117	1.45	0.77
		Ferritic	1.12	0.109	1.58	0.85
Minor axis bending plus axial compression	New proposal	Austenitic	1.29	0.15	1.78	0.87
		Duplex	1.20	0.14	1.91	0.81
		Ferritic	1.23	0.15	1.90	0.90
	EN 1993-1-2 [19]	Austenitic	1.10	0.25	2.32	0.64
		Duplex	1.17	0.257	2.24	0.59
		Ferritic	1.20	0.23	2.06	0.67

Table 6: Reliability assessment of new proposals against FE results relative to EN 1993-1-2 [19] for stainless steel beam-columns in fire

Loading condition	Design method	Grade	Criterion 1	Criterion 2	Criterion 3
Major axis bending plus axial compression	New proposal	Austenitic	0.00	6.98	-0.15
		Duplex	0.01*	11.82	-10.03
		Ferritic	0.00	6.73	-12.05
	EN 1993-1-2 [19]	Austenitic	7.73*	39.15*	-0.03
		Duplex	7.99*	33.76*	-4.05
		Ferritic	0.24*	14.90	-0.10
Minor axis bending plus axial compression	New proposal	Austenitic	0.00	6.00	-20.85
		Duplex	0.74*	11.08	-15.28
		Ferritic	0.00	7.78	-16.76
	EN 1993-1-2 [19]	Austenitic	23.50*	33.75*	-4.35
		Duplex	11.82*	31.77*	-9.36
		Ferritic	5.19*	22.88*	-12.53